

Global assessment of AMSR-E and MODIS cloud liquid water path retrievals in warm oceanic clouds

C. Seethala¹ and Ákos Horváth¹

Received 15 June 2009; revised 12 November 2009; accepted 4 January 2010; published 7 July 2010.

[1] We compared 1 year of Advanced Microwave Scanning Radiometer-EOS (AMSR-E) Wentz and Moderate Resolution Imaging Spectroradiometer (MODIS) cloud liquid water path estimates in warm marine clouds. In broken scenes AMSR-E increasingly overestimated MODIS, and retrievals became uncorrelated as cloud fraction decreased, while in overcast scenes the techniques showed generally better agreement, but with a MODIS overestimation. We found microwave and visible near-infrared retrievals being most consistent in extensive marine Sc clouds with correlations up to 0.95 and typical RMS differences of 15 g m^{-2} . The overall MODIS high bias in overcast domains could be removed, in a global mean sense, by adiabatic correction; however, large regional differences remained. Most notably, MODIS showed strong overestimations at high latitudes, which we traced to 3-D effects in plane-parallel visible-near-infrared retrievals over heterogeneous clouds at low Sun. In the tropics or subtropics, AMSR-E-MODIS differences also depended on cloud type, with MODIS overestimating in stratiform clouds and underestimating in cumuliform clouds, resulting in large-scale coherent bias patterns where marine Sc transitioned into trade wind Cu. We noted similar geographic variations in Wentz cloud temperature errors and MODIS $1.6\text{--}3.7 \mu\text{m}$ droplet effective radius differences, suggesting that microwave retrieval errors due to cloud absorption uncertainties, and visible near-infrared retrieval errors due to cloud vertical stratification might have contributed to the observed liquid water path bias patterns. Finally, cloud-rain partitioning was found to introduce a systematic low bias in Wentz retrievals above 180 g m^{-2} as the microwave algorithm erroneously assigned an increasing portion of the liquid water content of thicker nonprecipitating clouds to rain.

Citation: Seethala, C., and Á. Horváth (2010), Global assessment of AMSR-E and MODIS cloud liquid water path retrievals in warm oceanic clouds, *J. Geophys. Res.*, 115, D13202, doi:10.1029/2009JD012662.

1. Introduction

[2] The weakest link in climate simulations is the poor representation of clouds, particularly of marine boundary layer clouds, which constitute the main source of uncertainty in modeled cloud feedbacks [Bony and Dufresne, 2005]. The dominant part of predicted global cloud forcing change is produced by these ubiquitous warm clouds, the radiative fluxes of which are very sensitive to their vertically integrated liquid water content or liquid water path (LWP) [Turner et al., 2007]. Therefore, climate-modeling efforts would greatly benefit from accurate cloud LWP measurements with well-established error characteristics.

[3] The longest global climatologies of cloud LWP have been derived from spaceborne passive microwave and visible near-infrared (VNIR) observations. The microwave record now spans 20+ years and comprises Special Sensor Microwave/Imager (SSM/I), Tropical Rainfall Measurement

Mission Microwave Imager (TMI), and Advanced Microwave Scanning Radiometer for Earth Observing System (AMSR-E) measurements. High-quality VNIR LWP estimates, however, have only been available since the launch of the Moderate Resolution Imaging Spectroradiometer (MODIS) a decade ago.

[4] The de facto microwave retrieval standard is the Wentz algorithm developed by Remote Sensing Systems (RSS) [Wentz, 1997; Wentz and Spencer, 1998; Wentz and Meissner, 2000; Hilburn and Wentz, 2008]. RSS derives cloud liquid water path directly from brightness temperatures using essentially the same multichannel algorithm for SSM/I, TMI, and AMSR-E. VNIR LWPs, on the other hand, represent indirect estimates being parameterized from cloud optical thickness and droplet effective radius, which are retrieved from solar reflectances. The current state-of-the-art MODIS algorithm [Platnick et al., 2003] is an updated version of the classic Nakajima and King [1990] bispectral method.

[5] Unfortunately, neither satellite technique has been comprehensively validated. Comparisons with in situ and ground-based measurements, although useful in case studies,

¹Max Planck Institute for Meteorology, Hamburg, Germany.

suffer from representativeness and sample size issues as well as from significant biases in surface microwave retrievals [Turner *et al.*, 2007]. An alternative to episodic validation campaigns is the evaluation of the two fully independent satellite methods against each other using a large set of coincident retrievals. Several such studies have assessed Wentz and MODIS LWPs recently.

[6] In broken cloud fields the Wentz algorithm has been found to increasingly overestimate MODIS with decreasing cloud fraction [Bennartz, 2007; Horváth and Davies, 2007]. Analysis of cloud-free scenes has also indicated a Wentz overestimation, the magnitude of which decreases with surface wind speed and increases with column water vapor [Greenwald *et al.*, 2007; Horváth and Gentemann, 2007]. Taken together, these findings have strongly suggested potential beam-filling, surface emission, and gaseous absorption errors in the Wentz algorithm, although significant heterogeneity errors in MODIS retrievals could not be ruled out either.

[7] The techniques have been found considerably better correlated in overcast scenes, but with the opposite tendency of MODIS overestimations. Borg and Bennartz [2007] have shown that this positive MODIS bias could be eliminated, at least in a global mean sense, by replacing the operational vertically homogeneous cloud model with an adiabatically stratified one. However, even after adiabatic corrections, systematic differences remain, with AMSR-E increasingly underestimating MODIS for cloud optical thicknesses above ~ 20 [Wilcox *et al.*, 2009]. Some of these discrepancies might be due to assumptions about the partitioning of cloud water and rainwater in the Wentz algorithm, as pointed out by Horváth and Davies [2007] and O'Dell *et al.* [2008].

[8] These are important results, but more robust comparisons are needed because all previous studies had serious temporal or regional limitations. In this work, we performed a systematic global comparison of AMSR-E and MODIS LWP estimates from 1 year of data. Section 2 describes our satellite data sets and analysis methodology. Section 3 gives a detailed account of microwave-VNIR differences. Section 4 then discusses potential first-order error sources that might explain the observed biases. Finally, section 5 summarizes our findings.

2. Data and Methodology

[9] Our data set comprised cloud retrievals from AMSR-E and MODIS on the Aqua satellite, and near-simultaneous aerosol observations from the Ozone Monitoring Instrument (OMI) aboard the Aura platform, covering the period December 2006 to November 2007. Only high-quality retrievals were used from the latest available products: version 5 for AMSR-E, collection 5 for MODIS, and version 3 for OMI. In the following, we summarize the relevant aspects of each algorithm.

2.1. AMSR-E Wentz Cloud Liquid Water Path

[10] The Wentz algorithm is an absorption-emission-based method sequentially retrieving sea surface temperature (SST), surface wind speed (W), water vapor path (V), liquid water path (LWP), and rain rate (R), both day and night but only over the ocean. Our primary interest, LWP, is derived from 37 GHz observations at a resolution of 13 km,

but here we used the 0.25° gridded daytime product. These microwave LWPs can be interpreted as gridbox means (averages over clear sky and cloud) because the relationship between the 37 GHz retrievals and subfield-of-view cloud amount is nearly linear [Greenwald *et al.*, 1997; Lafont and Guillemet, 2004]. First, a preliminary value is computed assuming the atmospheric column contains only cloud liquid but no rain. Then, rain retrieval is performed for preliminary LWPs above a fixed rain-threshold of 180 g m^{-2} . Although this step concerns only $\sim 5\%$ of all data, it is a source of systematic error due to its built-in assumptions; therefore, it warrants a more detailed discussion.

[11] The simultaneous presence of cloud liquid and rain poses a fundamental challenge to *all* microwave methods and not only to the Wentz algorithm because the component signals cannot be separated from brightness temperatures alone. The basic microwave observable is total liquid water columnar attenuation A_{L37} . In the first pass through data, no rain is assumed and a preliminary LWP proportional to A_{L37} is retrieved. For a preliminary LWP $> 180 \text{ g m}^{-2}$, however, precipitation is diagnosed and the governing equation becomes [Hilburn and Wentz, 2008]

$$A_{L37} = a_{37}(1 - b_{37}\Delta T) \text{LWP}_R \times 10^{-3} + c_{37}(1 + d_{37}\Delta T) H R^{e_{37}} \quad (1a)$$

$$\Delta T = T_L - 283 \text{ K}. \quad (1b)$$

[12] Here a_{37} , b_{37} , c_{37} , d_{37} , and e_{37} are coefficients derived using the Marshall-Palmer raindrop size distribution, T_L is liquid cloud temperature in kelvins, H is rain column height in kilometers, R is column-average rain rate in millimeters per hour, and LWP_R is the rain-adjusted cloud liquid water path in millimeters. Cloud temperature is parameterized from SST and water vapor, while rain column height is fitted to freezing level heights from reanalysis data and varies linearly with SST from 0.46 km at 0°C to 5.26 km at 30°C . In order to solve equation (1) with two unknowns, LWP_R and R , the Wentz algorithm further assumes that cloud liquid water scales as the square root of rain rate [Hilburn and Wentz, 2008]

$$\text{LWP}_R = \alpha \left(1 + \sqrt{HR}\right), \quad (2)$$

where $\alpha = 180 \text{ g m}^{-2}$ is the rain threshold LWP. With equation (2) and the above parameterizations, equation (1) can now be solved for R . The resulting rain rate is then substituted back in equation (2) in order to obtain the final rain-adjusted cloud liquid water path replacing the preliminary rain-free value.

[13] This specific cloud-rain partitioning was derived from a study of northeast Pacific extratropical cyclones. Changing equation (2) or even the assumed raindrop size distribution would result in a different cloud-rain partitioning. The value of $\alpha = 180 \text{ g m}^{-2}$ was chosen because it yields good agreement between Wentz and other rain climatologies [Hilburn and Wentz, 2008]. From the perspective of LWP retrievals, however, use of a relatively low and globally fixed cloud-rain threshold entails underestimations whenever nonraining clouds with LWPs exceeding the threshold

are encountered because some of the cloud water is erroneously assigned to precipitation. As we show in section 4.5, this negative bias explains some of the observed discrepancies between Wentz and MODIS LWPs.

2.2. MODIS Cloud Liquid Water Path

[14] Here, cloud LWP is indirectly estimated from cloud optical thickness (τ) and droplet effective radius (r_e), themselves inferred from bispectral solar reflectances at 1 km resolution (MYD06 product). Over the ocean, MODIS uses the 0.86 μm visible band containing optical thickness information, in conjunction with one of three water-absorbing near-infrared bands located at 1.6, 2.2, and 3.7 μm , which are sensitive to the droplet effective radius. Although all three near-infrared channels generally observe the upper portion of clouds, vertical sampling of droplets becomes progressively deeper from 3.7 to 1.6 μm due to decreasing absorption [Platnick, 2000]. The operational LWP parameterization relies on the 2.2 μm band and assumes no vertical variation in cloud droplet size, leading to

$$\text{LWP} = \frac{4\rho_w}{3Q_e} \tau r_{e,2.2}, \quad (3)$$

where $Q_e \approx 2$ is the extinction efficiency at visible wavelengths and $\rho_w = 1 \text{ g cm}^{-3}$ is water density. (Note that LWP is only estimated when both τ and r_e retrievals are successful; the latter often fail in thin clouds leading to fewer LWP retrievals than cloudy pixels.) Presumed vertical homogeneity in combination with cloud top effective radius retrievals can lead to LWP biases of both signs depending on the actual droplet profile. For example, in the absence of τ and r_e retrieval errors, equation (3) would be an overestimate in marine Sc clouds, where the effective radius often increases linearly from cloud base to top. For such boundary layer clouds, an adiabatic model has been proposed based on cloud top effective radius $r_{e,\text{top}}$ [Wood and Hartmann, 2006]

$$\text{LWP} = \frac{10\rho_w}{9Q_e} \tau r_{e,\text{top}}. \quad (4)$$

[15] Theoretically, $r_{e,3.7}$ is closest to $r_{e,\text{top}}$; however, $r_{e,3.7}$ has an unexplained low bias (see section 4.3). In practice, therefore, $r_{e,2.2}$ is used in equation (4) as well, which reduces equation (3) by a factor of 5/6 or 17%. Because this model does not consider entrainment mixing, it represents only a first-order LWP correction in mostly subadiabatic marine Sc. In addition, when r_e decreases with height, which might occur in drizzling or raining clouds, equation (4) could even exacerbate the underestimation of equation (3). At least in theory, a better approach would be to estimate the droplet-size profile on a case-by-case basis from the three effective radii. Unfortunately, vertical weighting functions of the three MODIS near-infrared channels are quite similar and correlated, rendering droplet profile inversion questionable [Platnick, 2000]. Nevertheless, we show in section 4.3 that in certain geographic regions large-scale variations of microwave-VNIR LWP bias appear correlated with a 1.6–3.7 μm effective radius difference.

[16] Another significant error source in MODIS LWP estimates is the potential breakdown of the 1-D plane-

parallel radiative transfer used in the calculations [Horváth and Davies, 2004]. The impact of heterogeneity (3-D) effects on 1-D cloud optical thickness has been extensively studied, but that on the 1-D droplet effective radius has only been recently considered and is still rather uncertain [Marshak *et al.*, 2006]. Possible 3-D errors in VNIR LWP are also poorly known; we investigate such errors in section 4.1 by analyzing AMSR-E-MODIS retrieval differences as a function of horizontal cloud heterogeneity.

2.3. OMI Aerosol Index

[17] Because absorbing aerosols can apparently reduce MODIS LWP [Haywood *et al.*, 2004], we used the OMI ultraviolet Aerosol Index (AI) to identify areas affected by biomass smoke or desert dust, and estimated the resulting LWP retrieval bias in section 4.4. OMI AI represents the deviation of the measured 354 nm radiance from model calculations in a purely molecular atmosphere bounded by a Lambertian surface, and has the unique ability to detect aerosols above clouds [Torres *et al.*, 2007]. Specifically, we used the daily Level-2 gridded product (OMAERUVG) with values above 1 indicating substantial amounts of absorbing particles.

2.4. Comparison Methodology

[18] In this study, all higher-resolution retrievals were averaged down to the 0.25° scale of the regular AMSR-E grid. Performing the analysis on a microwave footprint-level as done by Greenwald *et al.* [2007] would have offered slightly more detailed error information; however, at the cost of a greatly increased computational burden and reduced data volume. Our choice was further motivated by climate model diagnostics strongly favoring the gridded Wentz product.

[19] Because microwave LWPs represented gridbox means but MODIS LWPs were in-cloud retrievals, the latter were multiplied by the gridbox-mean fraction of successful MODIS retrievals, henceforth referred to as “cloud fraction.” The presence of cloud top ice generally makes comparisons ambiguous due to different instrument sensitivities [Horváth and Davies, 2007]; therefore, we restricted our analysis to ice-free gridboxes as identified by the MODIS cloud phase product. In addition, we only considered nonprecipitating clouds with zero AMSR-E rain rates; the sole exception was section 4.5 discussing cloud-rain partitioning issues.

3. Bias Analysis

3.1. Clear-Sky Wentz Bias

[20] Before analyzing cloudy scenes we evaluated Wentz LWP retrievals in clear-sky conditions in order to gain some measure of their uncertainties. We only considered domains where all MODIS pixels were classified as confident clear, still obtaining more than three million samples. The global annual mean clear-sky LWP bias was $\sim 12 \text{ g m}^{-2}$ in good agreement with the 12–15 g m^{-2} found by Horváth and Gentemann [2007] and Bennartz [2007], but higher than either the 7 g m^{-2} obtained by Greenwald *et al.* [2007] or the 5 g m^{-2} estimated by Wentz [1997]. Seasonal and hemispheric variations were small (1–2 g m^{-2}), which was in contrast to Greenwald *et al.* [2007], whose results exhibited considerably larger hemispheric differences of

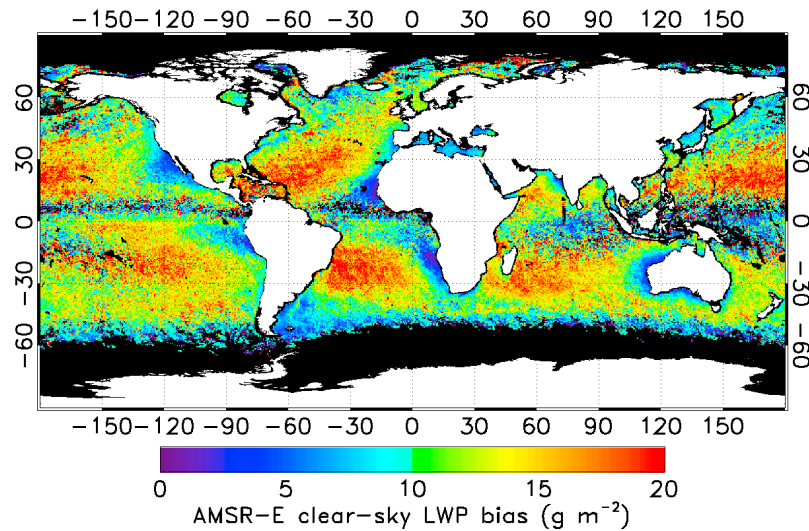


Figure 1. Geographic distribution of annual mean Advanced Microwave Scanning Radiometer-EOS (AMSR-E) clear-sky liquid water path (LWP) bias. In this and subsequent maps, black indicates no data.

12 g m⁻² for the north and 4 g m⁻² for the south; however, they only analyzed a 3 week period in July 2002, which might explain these discrepancies.

[21] Geographic variations were far more significant in our data set, as shown in Figure 1 for annual means. (Seasonal bias patterns were very similar.) We found the smallest clear-sky biases below 7 g m⁻² in extensive marine Sc regions as well as in the Mediterranean, Black Sea, Red Sea, and Persian Gulf. Warmer tropical or subtropical oceanic areas, on the other hand, exhibited the largest biases up to 20 g m⁻². These clear-sky biases most likely corresponded to uncertainties in the sea surface emissivity and water vapor and oxygen absorption models; however, cloud detection errors could not be ruled out. The global performance of the MODIS cloud mask is unknown, but in trade wind cumuli it has been shown to agree with a 15 m resolution cloud mask only 62% of the time [Zhao and Di Girolamo, 2006]. Thus,

cloud contamination might partly explain larger “clear-sky” LWPs in regions with frequent popcorn Cu.

[22] Cloud detection errors aside, one would prefer microwave-derived parameters to be independent of one another. Unfortunately, this is not the case, as demonstrated in Figure 2, where we plotted the mean clear-sky LWP bias binned according to surface wind speed, water vapor, and SST. We found a negative correlation with wind in all seasons and latitude bands, whereby the LWP bias decreased from 15 to 16 g m⁻² to 2–3 g m⁻² as wind increased from 0 to 15 m/s. Dependence on water vapor was generally weaker and more variable. In drier conditions ($V < 22$ mm) the LWP bias increased, while in wetter conditions ($V > 22$ mm) decreased or leveled off with vapor amount. The influence of SST was even more variable and was overall the weakest, except maybe in the warmest regions above 28°C, where the bias rapidly decreased.

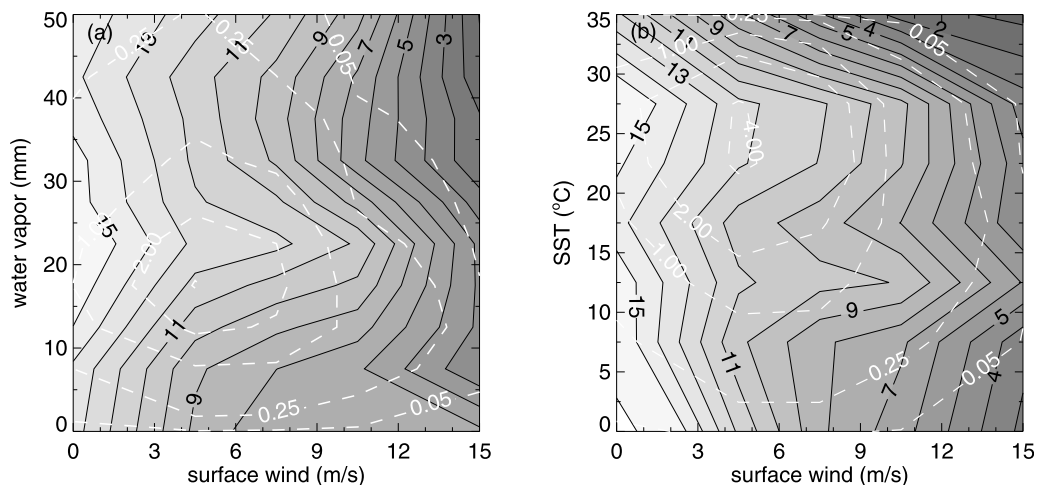


Figure 2. Annual mean AMSR-E clear-sky LWP bias binned according to (a) surface wind and column water vapor and (b) surface wind and sea surface temperature (SST). Solid black lines are LWP bias contours at 1 g m⁻² intervals, while dashed white lines indicate data frequency ($\times 10^5$).

Table 1. Global Annual Statistics of AMSR-E Wentz and MODIS LWP Retrievals in Warm Nonprecipitating Marine Clouds for Three Liquid Cloud Fraction Ranges^a

	All Domains (LCF = 0%–100%)		Overcast Domains (LCF = 95%–100%)		Broken Domains (LCF = 0%–50%)	
	Standard	Adiabatic	Standard	Adiabatic	Standard	Adiabatic
AMSR-E mean	58	58	91	91	44	44
MODIS mean	40	33	109	90	13	11
Bias	18	25	–18	1	31	33
Rms	41	36	38	31	35	35
Correlation	0.74	0.72	0.83	0.83	0.45	0.45
Sample number	6.1E+7		1.1E+7		3.6E+7	

^aMeans, biases (AMSR-E–MODIS), and RMS differences are given in g m^{-2} .

[23] These results were qualitatively consistent with findings by *Greenwald et al.* [2007] and indicated possible shortcomings in the surface emission and gaseous absorption models of the Wentz algorithm. We emphasize that while these clear-sky uncertainties might also be representative of low cloud fraction scenes, it is not obvious how they relate to retrieval errors in highly cloudy domains. Undoubtedly, more work is needed to understand and remove these unwanted interdependencies in clear-sky observations. Henceforth, we focus on cloud retrievals.

3.2. Global Annual Mean Statistics

[24] Annual statistics of AMSR-E and MODIS LWPs in ice- and rain-free domains, totaling more than 60 million retrievals, are summarized in Table 1. When all liquid cloud fractions (LCFs) were considered, AMSR-E overestimated MODIS by 18 g m^{-2} with respective means of 58 and 40 g m^{-2} . The data sets were moderately correlated with a coefficient of 0.74 and root-mean square (RMS) difference of 41 g m^{-2} , which was larger than the 25 g m^{-2} random error estimated by *Wentz* [1997] for microwave retrievals. Adiabatic correction made the overall comparison worse by further reducing MODIS LWPs and increasing the bias to 25 g m^{-2} .

[25] In overcast domains, defined as $\text{LCF} = 95\%–100\%$ and constituting 18% of all samples, LWP was significantly higher with means of 91 and 109 g m^{-2} for AMSR-E and MODIS, respectively. However, the bias was of opposite sign, as MODIS overestimated AMSR-E by 18 g m^{-2} . The agreement between the techniques was considerably tighter with an increased correlation of 0.83 . Adiabatic correction almost completely removed the MODIS overestimation resulting in a bias of only 1 g m^{-2} and RMS difference of 31 g m^{-2} . This corroborated *Bennartz* [2007] that the adiabatic cloud model is superior to the operational vertically homogeneous one, at least in a global mean sense.

[26] The above results suggested significantly higher microwave LWPs in broken clouds, which was confirmed by statistics for clear-sky dominated regions with $\text{LCF} < 50\%$. In this category, constituting 59% of all samples, AMSR-E and MODIS estimates were rather poorly correlated at 0.45 and showed the largest biases of $31–33 \text{ g m}^{-2}$ due mostly to a steep drop in the MODIS mean. Obviously, adiabatic corrections made matters worse for such broken scenes. Motivated by these findings, we further investigated the cloud fraction dependence of microwave–VNIR consistency in section 3.4. First, however, we discuss seasonal variations in global mean LWP.

3.3. Seasonal Variations in Global Means

[27] The month-to-month variation of AMSR-E and MODIS global mean LWPs is shown in Figure 3. Here black corresponds to AMSR-E, while red and green refer to standard and adiabatic MODIS, respectively. When all domains were considered, AMSR-E systematically overestimated MODIS similarly to the annual mean. The AMSR-E seasonal cycle had a minimum in December (54 g m^{-2}) and a single maximum in August (63 g m^{-2}). Standard MODIS also had a minimum in December (38 g m^{-2}); however, it had double maxima in March (42 g m^{-2}) and August (41 g m^{-2}). The resulting bias varied from 15 to 22 g m^{-2} with a minimum in March and a maximum in August. (The bias increased by a further $\sim 7 \text{ g m}^{-2}$ for adiabatic MODIS values.)

[28] By contrast, overcast means showed standard MODIS overestimation in all months. Here, seasonal cycles were in better qualitative agreement with both data sets with having a minimum in December (102 vs. 86 g m^{-2}) and double maxima in April (120 vs. 94 g m^{-2}) and August (110 vs. 95 g m^{-2}). For MODIS, however, the relative strengths of maxima were markedly different, and the amplitude of the seasonal cycle was larger. Adiabatic correction lowered MODIS values to within 5 g m^{-2} (or 6%) of

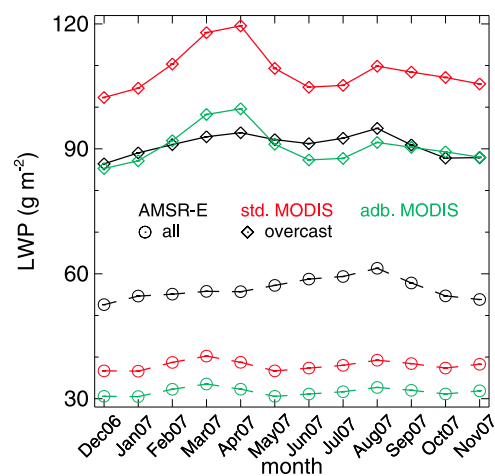


Figure 3. Seasonal variation of AMSR-E and Moderate Resolution Imaging Spectroradiometer (MODIS) global mean cloud LWP in warm nonprecipitating marine clouds for all domains (circles) and overcast domains (diamonds). Black, red, and green correspond to AMSR-E, standard (std.) MODIS, and adiabatic (adb.) MODIS, respectively.

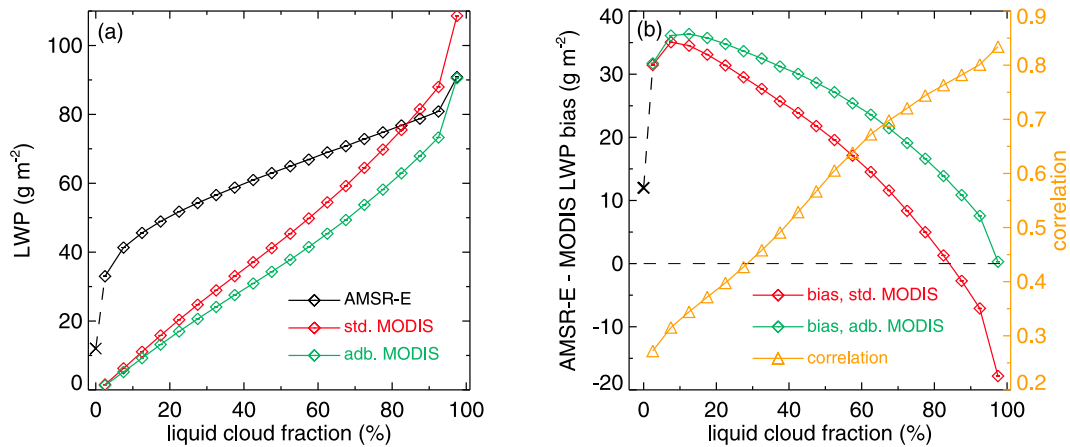


Figure 4. Liquid cloud fraction dependence of (a) AMSR-E and MODIS LWP and (b) the corresponding AMSR-E-MODIS bias and correlation for warm nonprecipitating marine clouds. The cross indicates the clear-sky background bias in AMSR-E LWP.

AMSR-E estimates, confirming its overall validity on monthly time scales as well.

3.4. Cloud Fraction Dependence

[29] Here we further investigate the strong dependence of microwave-VNIR comparison on scene brokenness. Mean AMSR-E and MODIS cloud LWPs are plotted for 5% wide liquid cloud fraction bins in Figure 4a. Standard MODIS means rapidly increased from 2 to 108 g m^{-2} , while AMSR-E means, varying from 33 to 91 g m^{-2} , were usually higher and showed a slower increase with cloud fraction. The corresponding bias steadily increased from -17 to $+35 \text{ g m}^{-2}$ as cloud fraction decreased, changing sign at an LCF of $\sim 80\%$ (see Figure 4b). Simultaneously, the correlation quickly dropped from 0.83 to 0.27, indicating poor correspondence between the techniques in highly broken scenes. (Similar results were obtained regardless of view zenith angle or potential sunglint contamination.) These findings qualitatively agreed with Horváth and Davies [2007] and Horváth and Gentemann [2007] and showed adiabatic improvement only for cloud fractions above 90%.

[30] What could possibly cause such behavior? Plane-parallel MODIS retrievals are certainly subject to 3-D effects in broken clouds; however, the resulting biases in 1-D optical thickness and droplet effective radius are often of opposite sign, leading to partial cancellation of errors in 1-D LWP. Overall, shadowing dominates brightening, producing substantial r_e overestimations and somewhat smaller τ underestimations and hence a positive LWP bias [Marshak *et al.*, 2006; Evans *et al.*, 2008]. Indeed, Cornet *et al.* [2005] has found MODIS domain-mean LWP overestimating the 3-D value by 15% in a broken Sc scene off California. These studies suggest that 3-D errors in MODIS retrievals would go the wrong way in explaining the observed LWP bias in broken clouds.

[31] Another possibility is microwave beam-filling effects. The Wentz algorithm does not apply beam-filling corrections to rain-free observations, but we made an equivalent first-order correction by scaling MODIS LWPs with the successful cloud-retrieval fraction. This could lead to a MODIS low bias if cloud amounts were systematically underestimated in broken scenes. Although the MODIS

cloud mask is designed to screen conservatively, the findings of Zhao and Di Girolamo [2006] have indicated that it tends to overestimate cloud fraction in scattered clouds. On the other hand, the fraction of successful MODIS LWP retrievals is usually less than the cloud fraction due to failed r_e retrievals, especially at low LWP. Therefore, uncertainties in cloud-amount scaling can potentially contribute to the observed biases.

[32] A more likely explanation, however, is reduced microwave sensitivity to low LWPs at 37 GHz, which makes retrievals in broken clouds rather susceptible to water vapor absorption and surface emission uncertainties. In section 3.1, we found a residual microwave clear-sky bias negatively correlated with surface wind and positively with water vapor. Cloud LWP bias showed similar dependencies, particularly at lower cloud amounts: AMSR-E overestimation decreased with wind speed and increased with water vapor. In addition, the older gaseous absorption and liquid dielectric models of the Wentz algorithm have been shown by Zuidema *et al.* [2005] to cause LWP overestimations compared to more recent models. All this suggests that updated surface emission and atmospheric absorption parameterizations might reduce the disagreement between Wentz and MODIS LWPs at the low end of the distribution; however, improved MODIS cloud fraction estimates might also have a positive impact.

3.5. Zonal Means

[33] Henceforward, we focus on overcast clouds because in broken cloud scenes the dominant AMSR-E overestimation makes analysis of other error sources difficult. Figure 5 plots the zonal variation of AMSR-E and MODIS LWP (Figures 5a–5c), and that of the resulting bias (Figures 5d–5f), separately for annual, boreal summer, and boreal winter periods. Annual results showed the LWP peak of the Intertropical Convergence Zone (ITCZ) in both data sets, somewhat more strongly in AMSR-E than MODIS. Microwave zonal means had additional midlatitude maxima, more markedly in the Southern Hemisphere. The most striking difference between the techniques occurred poleward of 40° , where AMSR-E LWP generally decreased but MODIS LWP strongly increased. Overall, standard MODIS

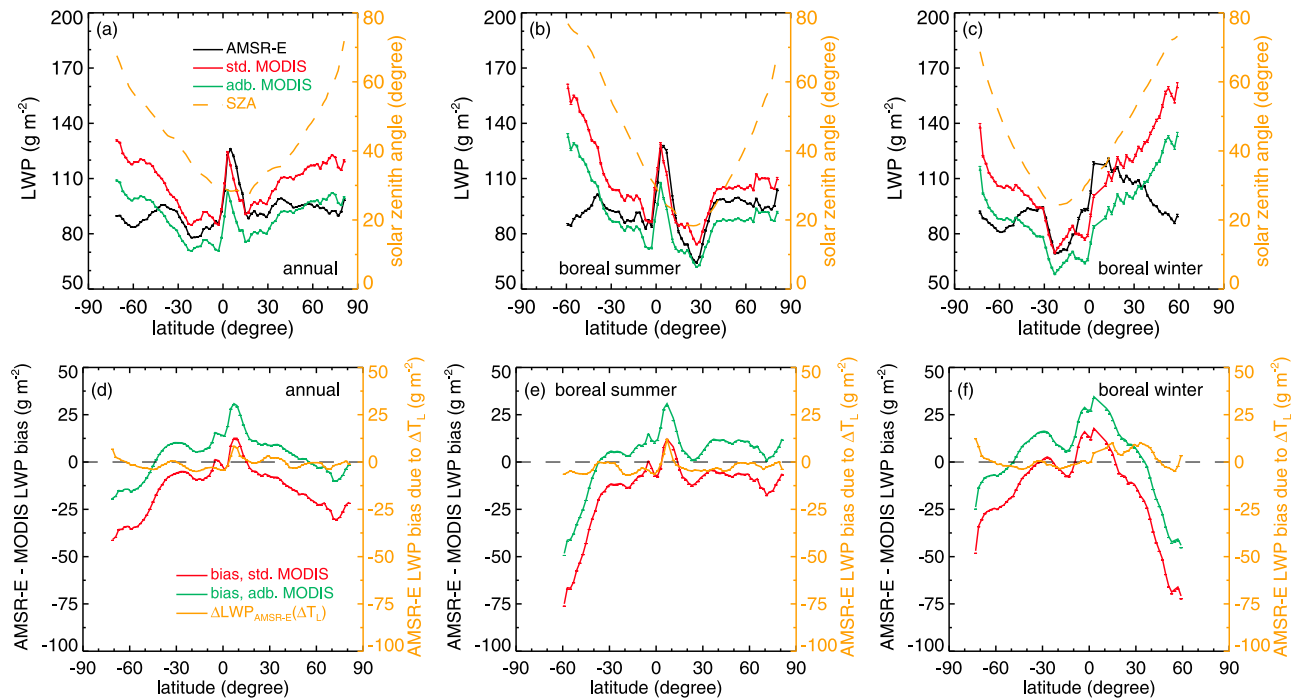


Figure 5. (a–c) Annual, boreal summer, and boreal winter zonal mean AMSR-E LWP (black), standard MODIS LWP (red), and adiabatic MODIS LWP (green) in overcast domains of warm nonprecipitating marine clouds. Dashed orange line is solar zenith angle (SZA). (d–f) Corresponding AMSR-E–MODIS LWP bias. Orange line indicates estimated AMSR-E LWP bias due to cloud temperature errors assuming a 3%/K sensitivity (see Figure 9). Bars depict the standard error of the mean.

overestimated AMSR-E in most regions and increasingly so toward the poles, with the exception of northern equatorial areas, where AMSR-E was slightly larger. The results also indicated that the negligible global mean bias between microwave and adiabatic VNIR estimates was due to cancellation of errors: adiabatic MODIS underestimated AMSR-E between 45°S and 45°N and overestimated it at higher latitudes.

[34] Comparing seasonal results yielded some clues regarding the cause of the strong poleward increase in MODIS LWP. In boreal summer, the qualitative agreement between AMSR-E and MODIS was reasonably good in the Northern Hemisphere, including middle to high latitudes. However, in the Southern Hemisphere MODIS showed a very rapid increase poleward of 30°S in contrast to AMSR-E. The situation was approximately reversed in boreal winter, when the largest MODIS overestimations occurred in the Northern Hemisphere poleward of 30°N, although biases were rather large in the Southern Hemisphere as well. In sum, the largest zonal differences occurred at high latitudes in the winter hemisphere.

[35] These large discrepancies cannot be explained by AMSR-E LWP biases caused by Wentz cloud temperature errors, as shown by the orange lines in Figures 5d–5f (see also section 4.2). However, in section 4.1 we offer evidence that they were the likely result of MODIS LWP overestimations due to 3-D retrieval errors in heterogeneous clouds at low Sun.

3.6. Global Distribution of Bias

[36] Because zonal means can mask large regional differences, we extended the bias analysis to the full globe.

Geographic variation of annual mean AMSR-E–standard MODIS LWP bias is mapped in Figure 6a for overcast domains. The strong zonal variation of the bias was evident here as well (compare Figure 5d). Poleward of 40°, MODIS consistently and increasingly overestimated AMSR-E at all longitudes. In the tropics/subtropics (30°S–30°N), however, large regional differences occurred corresponding to varying cloud regimes. In extensive marine Sc regions, MODIS showed significantly higher values, while in areas where cumuliform clouds were more frequent, AMSR-E LWPs were larger. This produced large-scale coherent bias gradients wherever marine Sc transitioned into mostly convective cloud regimes, with the two most notable areas being the tropical eastern/southeast Pacific and Gulf of Guinea/southeast Atlantic.

[37] In the first region, marine Sc forming over the cold Peru Current showed AMSR-E–standard MODIS LWP biases of -15 to -30 g m^{-2} . This region of negative bias also included the Pacific Cold Tongue. Parallel to its northern edge ran an equally narrow band of positive LWP biases (up to $+30$ g m^{-2}), producing sharp zonal gradients in this region. A similar but more extensive LWP bias pattern occurred in the southeast Atlantic off the African coast. Here higher standard MODIS LWPs in marine Sc developing over the cold Benguela Current smoothly transitioned into higher AMSR-E LWPs in the more cumuliform clouds of the Gulf of Guinea.

[38] The bias map for adiabatically corrected MODIS is plotted in Figure 6b. Adiabatic correction reduced the bias wherever standard MODIS overestimation was higher than 8%. (The black line delineates the border between adiabatic

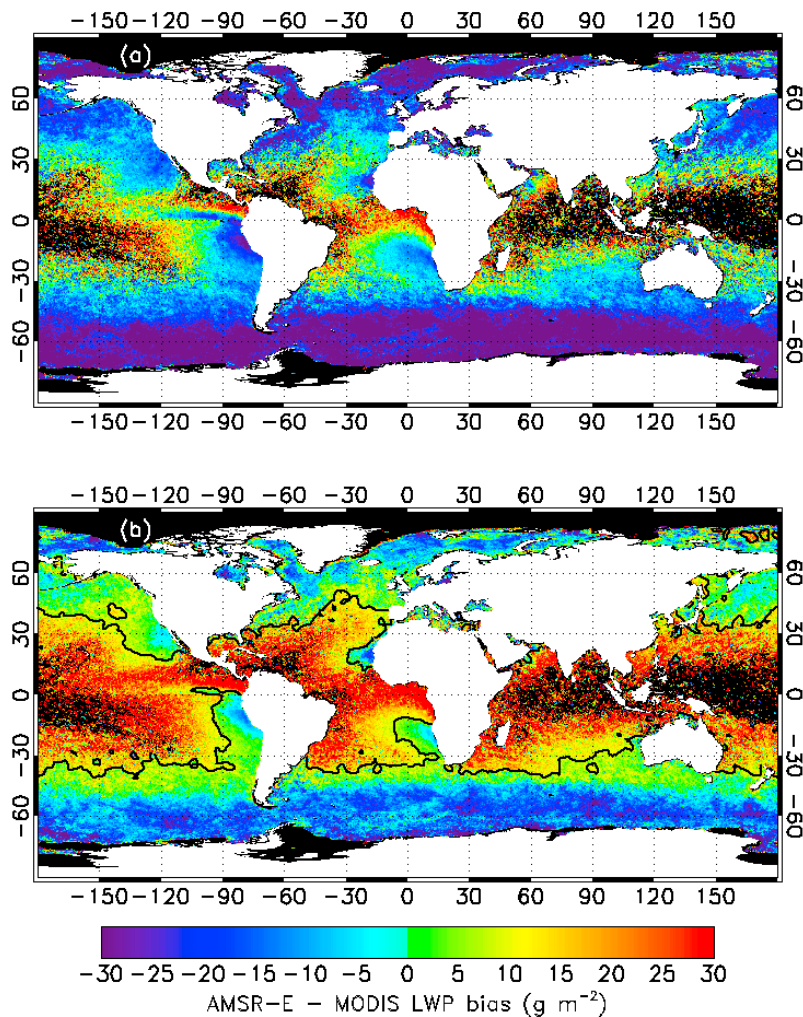


Figure 6. Annual AMSR-E-MODIS LWP bias map in overcast situations for (a) standard and (b) adiabatic visible near-infrared (VNIR) model. The black line marks the boundary between adiabatic improvement and deterioration.

improvement and deterioration.) These areas were primarily mid- to high-latitude oceans poleward of 40° but also included low-latitude marine Sc regions. Within the tropics/subtropics, however, adiabatic correction mostly increased the AMSR-E-MODIS LWP bias. Overall, we found that adiabatic LWP was an improvement over standard LWP in 75% of individual MODIS retrievals. In this data subset, the standard MODIS high bias of 23 g m^{-2} reduced to 5 g m^{-2} after the correction. In the remaining quarter of data, on the other hand, the AMSR-E high bias increased from ~ 0 to 16 g m^{-2} . When averaging over all data, this eliminated the global mean standard MODIS high bias of 18 g m^{-2} (see Table 1).

[39] Finally, we investigated geographic variations in the correlation and RMS difference between AMSR-E and MODIS LWPs, as illustrated in Figure 7. Overall, the data sets were correlated at 0.83 with an RMS of 38 g m^{-2} but regional differences were nonnegligible. The lowest correlations (down to 0.75) and largest RMS differences (up to and above 55 g m^{-2}) were found mostly at high latitudes above 55° – 60° , especially in the Northern Hemisphere, for

example, Hudson Bay, James Bay, and the areas surrounding the Labrador Peninsula and Newfoundland. Encouragingly, the correspondence between the techniques was excellent in marine Sc regions with correlations up to 0.95 and typical RMS differences of only 10 – 20 g m^{-2} , albeit with a systematic MODIS overestimation as shown before.

4. Potential Error Sources

4.1. Heterogeneity Effects in MODIS LWP

[40] As shown previously, a strong feature of AMSR-E-MODIS LWP differences was an increasing MODIS overestimation at higher latitudes poleward of 40° . These latitudes are generally observed at lower Sun (see Figure 5) suggesting that different solar zenith angle (SZA) dependencies of microwave and VNIR retrievals might contribute to the observed discrepancies. Indeed, previous studies found systematic SZA-dependent biases in 1-D plane-parallel cloud optical thickness retrievals. Based on Earth Radiation Budget Satellite observations, *Loeb and Davies [1996]* noted an increasing overestimation in nadir-view

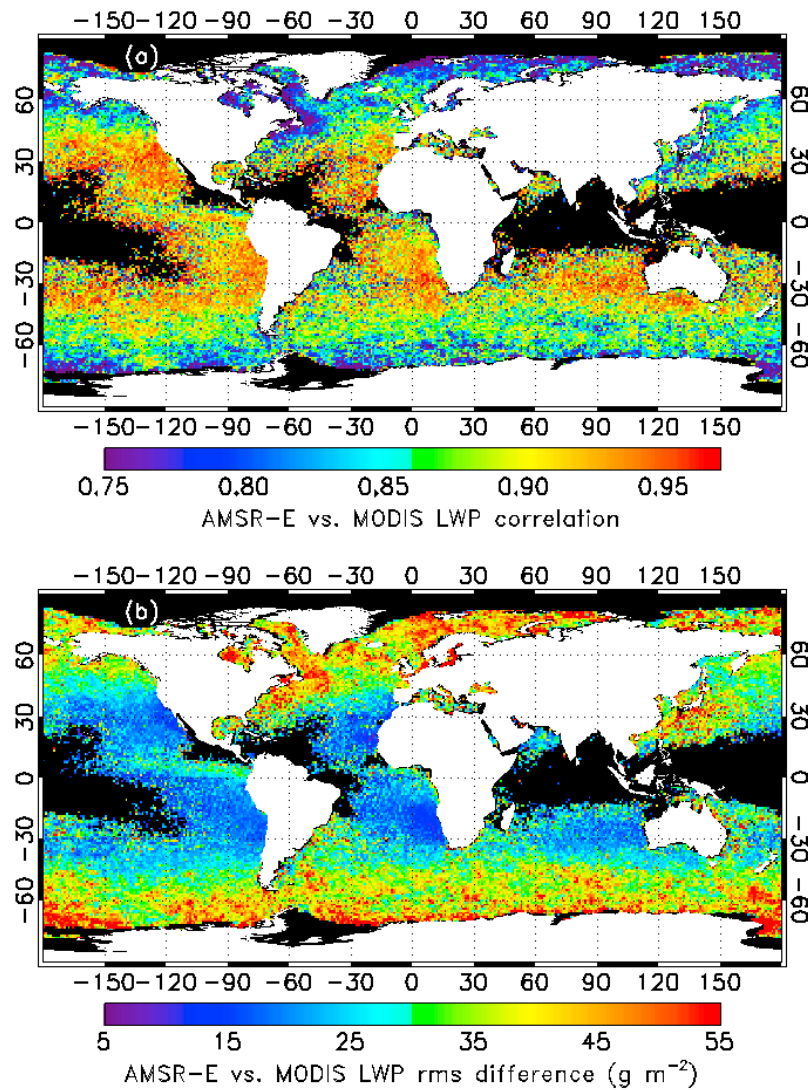


Figure 7. (a) Annual AMSR-E versus standard MODIS LWP correlation and (b) RMS difference map for overcast domains. Shown results are above the 99% confidence limit.

cloud optical thickness at higher SZAs, particularly above 60° . *Loeb and Coakley* [1998] obtained similar results in advanced very high-resolution radiometer (AVHRR) measurements even for marine Sc, which is arguably the closest to being plane-parallel.

[41] The strong increase in optical thickness was traced back to the fact that plane-parallel model reflectances, on average, decreased with SZA, while observed reflectances increased. The hypothesis that this discrepancy was due to neglected 3-D effects, such as cloud side illumination and bumpy cloud tops, was later confirmed through Monte Carlo simulations by *Loeb et al.* [1998] and *Várnai and Marshak* [2001]. The above studies only considered near-nadir views; however, *Várnai and Marshak* [2007] found similarly strong SZA-dependent increases in MODIS cloud optical thickness at all view angles.

[42] Motivated by these findings, we analyzed AMSR-E and MODIS LWPs as a function of SZA and scene heterogeneity. Heterogeneity of a 0.25° domain was characterized by *Cahalan et al.*'s [1994] χ parameter, defined as the ratio

of the logarithmic and linear average of 1 km cloud optical thicknesses. In general, χ varies from 0 to 1, with larger values indicating less heterogeneity; for the overcast domains considered in our analysis it ranged from 0.7 to 1.0. A detailed analysis of cloud heterogeneity from MODIS is deferred to *Oreopoulos and Cahalan* [2005]; however, two caveats are worth noting here. First, the χ parameter cannot distinguish if heterogeneity is due primarily to cloud top height or cloud extinction variations. Second, it measures “apparent” cloud heterogeneity because it is calculated from plane-parallel retrievals, which are themselves affected by 3-D effects. Consequently, χ may overestimate “true” heterogeneity in cases with significant shadowing and side illumination.

[43] The SZA dependence of AMSR-E and MODIS LWP is shown in Figures 8a and 8b for four χ bins of increasing homogeneity (red, green, and blue in Figure 8a and orange in Figure 8b). Up to a SZA of $\sim 35^\circ$, microwave and VNIR estimates were in relatively good agreement, both exhibiting modest increases, which most likely represented zonal var-

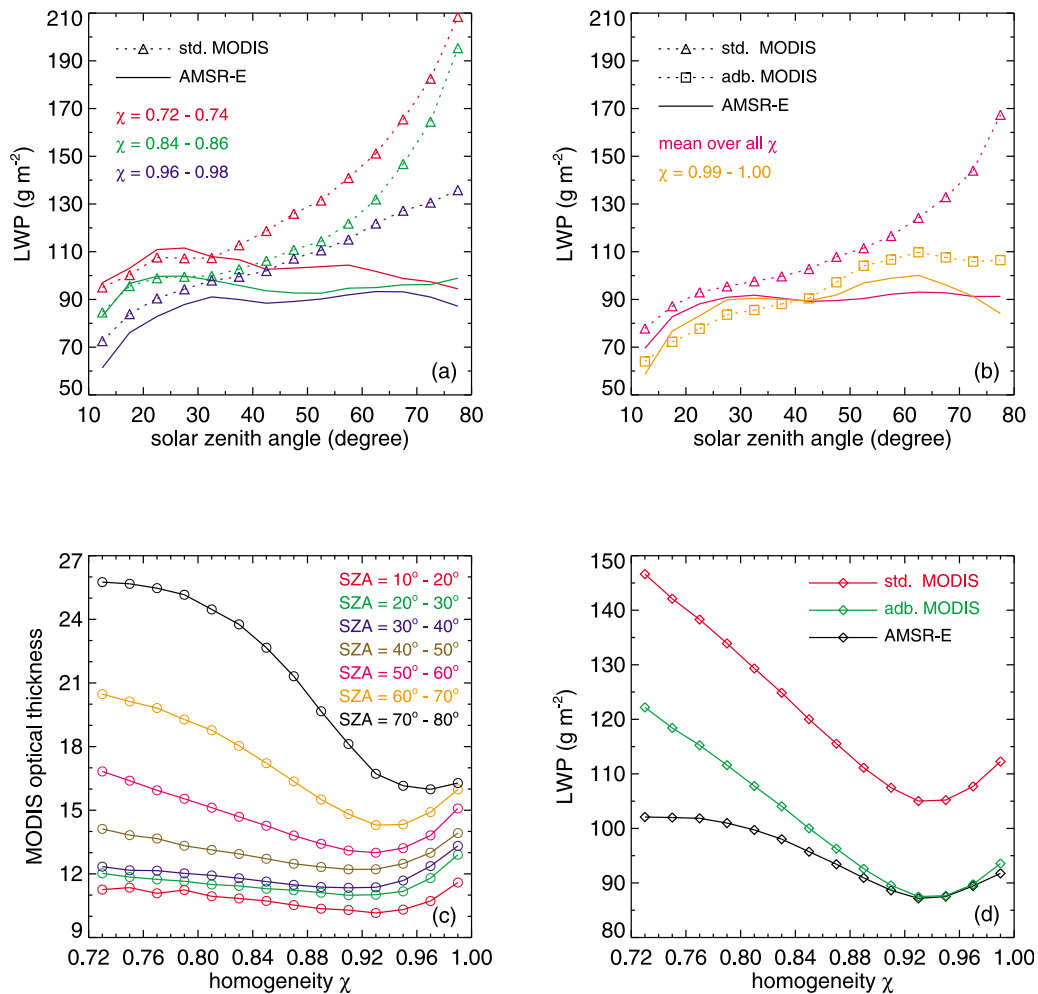


Figure 8. (a–b) SZA dependence of MODIS and AMSR-E LWP for various homogeneity classes, (c) MODIS cloud optical thickness versus scene homogeneity for (c) different SZA ranges and (d) mean (average over all SZAs) MODIS and AMSR-E LWP versus scene homogeneity. Results are for warm nonprecipitating overcast domains with χ calculated at the 0.25° scale.

iations in LWP. At higher SZAs, however, they showed strikingly different behavior. While AMSR-E LWP leveled off or even slightly decreased with SZA, MODIS LWP rapidly increased. The MODIS LWP increase was largest and nonlinear in SZA for the most heterogeneous scenes. As homogeneity increased, the MODIS LWP rise gradually became smaller and more linear with SZA. Only in the most homogeneous clouds ($\chi = 0.99 - 1.00$) did MODIS LWP level off with SZA, *qualitatively* similarly to AMSR-E LWP; these clouds were overwhelmingly marine Sc; thus, adiabatic correction to MODIS also resulted in good *quantitative* agreement between VNIR and microwave estimates (orange curve in Figure 8b). The SZA dependencies of mean LWPs averaged over all χ bins are given by the magenta curves in Figure 8b. As before, AMSR-E and MODIS LWPs started to diverge for $\text{SZA} > 35^\circ$, reaching a maximum MODIS overestimation of $\sim 80 \text{ g m}^{-2}$, or $\sim 90\%$ of the AMSR-E value, at the most oblique Sun. (Restricting the analysis to fixed geographic locations, thereby eliminating zonal variations, yielded similar differences between AMSR-E and MODIS SZA dependencies.)

[44] Our calculations confirmed optical thickness as the primary driver of the MODIS LWP rise with SZA. Up to a SZA of 35° , cloud optical thickness retrievals remained remarkably consistent irrespective of scene heterogeneity. At higher SZAs, however, optical thickness rapidly increased, especially in heterogeneous scenes. For example, between overhead and oblique Sun, τ varied from 11 to 16 in the most homogeneous clouds and from 11 to 28 in the most heterogeneous clouds. Droplet effective radius, on the other hand, showed a considerably smaller increase in the $11\text{--}13.5 \mu\text{m}$ range.

[45] Figure 8a also indicated a general decrease in both MODIS and AMSR-E LWP with increasing homogeneity, which we investigated in more detail. The variation of MODIS τ with homogeneity is plotted in Figure 8c for different SZA ranges. In accordance with our previous findings, τ systematically increased with SZA for all homogeneity values. However, at high Sun cloud optical thickness varied relatively weakly with χ , while at oblique Sun retrievals became very sensitive to scene heterogeneity. An interesting general pattern emerged whereby cloud

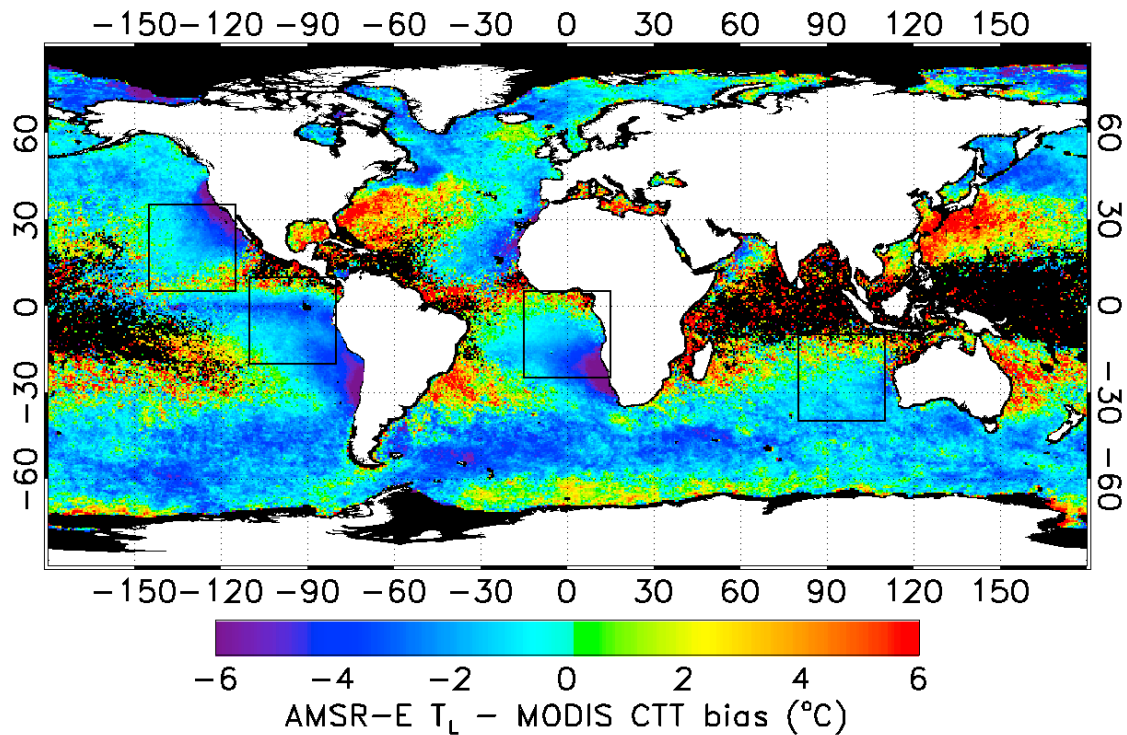


Figure 9. Annual bias between AMSR-E liquid cloud temperature (T_L) parameterization and MODIS cloud top temperature (CTT) measurements for warm nonprecipitating overcast domains. The relationship between LWP bias and cloud temperature bias in the four marked subregions is plotted in Figure 10.

optical thickness first decreased with increasing homogeneity, reaching a minimum value at $\chi \approx 0.93$, then it started to increase for even more homogeneous clouds. In essence, this figure summarizes our findings, which are as follows (1) heterogeneity effects are most important at oblique Sun (maybe above a SZA of 50°) and (2) the increase in optical thickness with SZA is significantly larger for heterogeneous than for homogeneous clouds.

[46] Finally, Figure 8d depicts the overall variation of AMSR-E and MODIS LWP with cloud homogeneity, averaged for all Sun elevations. Both LWP estimates exhibited qualitatively similar behavior, suggesting that the general τ - χ dependence in Figure 8c was due to the nature of clouds and not 3-D effects. However, MODIS retrievals were significantly more sensitive to scene heterogeneity than AMSR-E retrievals. In addition, standard MODIS overestimated AMSR-E by an increasing amount as heterogeneity increased. We found that in relatively homogeneous scenes, adiabatic correction could remove the mean MODIS overestimation almost entirely, resulting in excellent agreement between microwave and VNIR estimates for $\chi > 0.87$. Although the adiabatic model reduced VNIR LWP biases in more heterogeneous clouds as well, here corrections exceeding adiabatic would have been needed to fully compensate for the large MODIS 3-D-effect overestimations at low solar elevations.

4.2. Cloud Temperature Errors in AMSR-E LWP

[47] AMSR-E LWPs are sensitive to the assumed liquid temperature because microwave absorption is stronger in colder than in warmer clouds. Therefore, underestimation of

cloud temperature, that is, overestimation of absorption, implies an underestimation in microwave LWP, and vice versa. Earlier versions of the Wentz algorithm specified liquid cloud temperature T_L simply as the mean temperature between the sea surface and the freezing level, the current algorithm, however, uses a parameterization based on column water vapor and SST [Wentz and Meissner, 2000; Hilburn and Wentz, 2008]. O'Dell *et al.* [2008] investigated the errors in T_L by using temperature and cloud profiles from the European Centre for Medium-Range Weather Forecasts (ECMWF) global model. Compared to this model, they found a negative global mean bias of -1°C and an RMS error of 5°C in the Wentz parameterization, which, they estimated, would translate to an LWP low bias and RMS error of $\sim 3\%$ and $\sim 13\%$, respectively.

[48] In this work, we evaluated the Wentz T_L parameterization against MODIS cloud top temperature (CTT) retrievals. In good agreement with O'Dell *et al.* [2008], we found a global annual mean temperature bias of -1.5°C and an RMS error of $5^\circ\text{--}6^\circ\text{C}$ in T_L . The bias was somewhat smaller in boreal winter (-1.2°C) and spring (-1.2°C), and larger in boreal summer (-2.0°C) and fall (-1.8°C), with an absolute minimum in March (-1°C) and maximum in July (-2°C). Although these global mean biases were relatively small, they resulted from partial cancellation of significantly larger regional differences as demonstrated in Figure 9 for annual results. Over cold oceans, AMSR-E cloud temperature was generally underestimated with the largest errors, up to and beyond -6°C , occurring in marine Sc regions; this indicated that the current T_L parameterization did not adequately account for the temperature inversion associated with

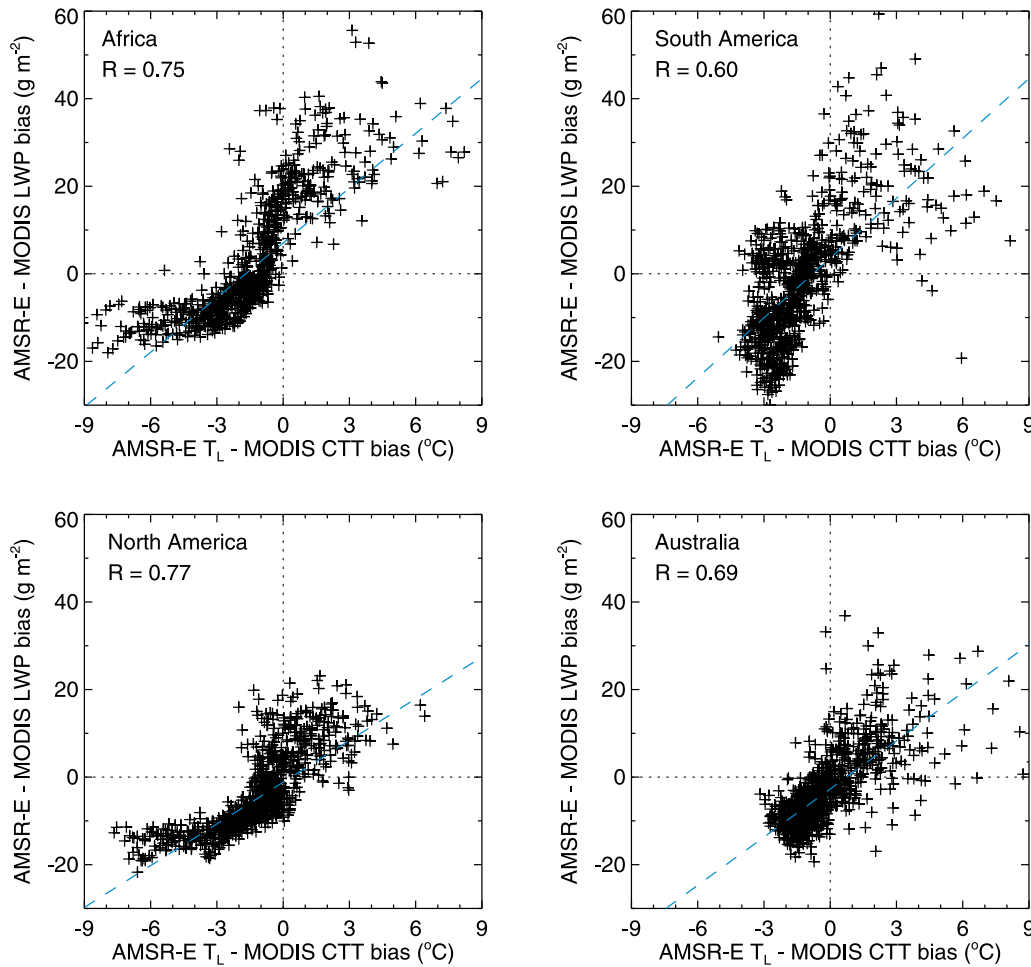


Figure 10. AMSR-E-standard MODIS LWP bias versus AMSR-E T_L -MODIS CTT bias in the four marked regions of Figure 9. Data are 1° annual means in warm nonprecipitating overcast clouds, and the correlation coefficients and dashed lines correspond to linear fits.

these clouds. In contrast, AMSR-E cloud temperature was overestimated by a similar amount above warm ocean currents (Kuroshio and Brazil Current, Gulf Stream), reflecting the SST dependence of the Wentz parameterization.

[49] Comparison of Figures 6 and 9 suggested that large-scale LWP bias variations might have been partly related to similar variations in cloud temperature error, particularly in marine Sc transition regions. In order to demonstrate this, we selected four such areas marked by black boxes in Figure 9: Africa (25°S – 5°N , 15°W – 15°E), South America (20°S – 10°N , 110°W – 80°W), North America (5°N – 35°N , 145°W – 115°W), and Australia (40°S – 10°S , 80°E – 110°E). Fortunately, the strong SZA-dependent MODIS overestimation, which was the dominant bias at higher latitudes/SZAs, was reduced in these low-latitude/SZA areas. Scatterplots of 1° annual mean AMSR-E, standard MODIS LWP bias versus AMSR-E T_L , and MODIS CTT bias are given in Figure 10.

[50] In all four regions, LWP bias and cloud temperature bias showed moderately strong positive correlations. The relationship was tightest in North America and Africa, the latter even suggesting a nonlinear relationship between the quantities, as indicated by a considerably higher rank correlation of 0.91. Everything else being equal, a negative

liquid temperature bias should cause a negative microwave LWP bias and vice versa. In broad agreement with this expectation, AMSR-E LWP mostly underestimated/overestimated MODIS LWP below/above a cloud temperature error of $-1^\circ\text{C}/0^\circ\text{C}$, but clearly additional effects were at play as well. The absolute LWP biases in Figure 10 corresponded to relative biases of $\pm 20\%$. If one uses *O'Dell et al.*'s [2008] sensitivity estimate of $\sim 3\%/^\circ\text{C}$, temperature errors of $\pm 6^\circ\text{C}$ would yield relative AMSR-E LWP errors of similar magnitude. The actual temperature sensitivity of operational Wentz LWPs will be quantified in a future study, by replacing the existing T_L parameterization with MODIS cloud top temperatures.

4.3. Cloud Vertical Stratification in MODIS LWP

[51] A potentially significant error source in VNIR LWP retrievals is neglecting cloud vertical stratification. As explained in section 2.2, the standard MODIS parameterization assumes a constant r_e throughout the cloud. Because the water-absorbing MODIS channels favorably sample toward cloud top, this might lead to both negative and positive LWP biases depending on the actual effective radius profile. The adiabatic parameterization constitutes a first-order correction in marine Sc often characterized by r_e

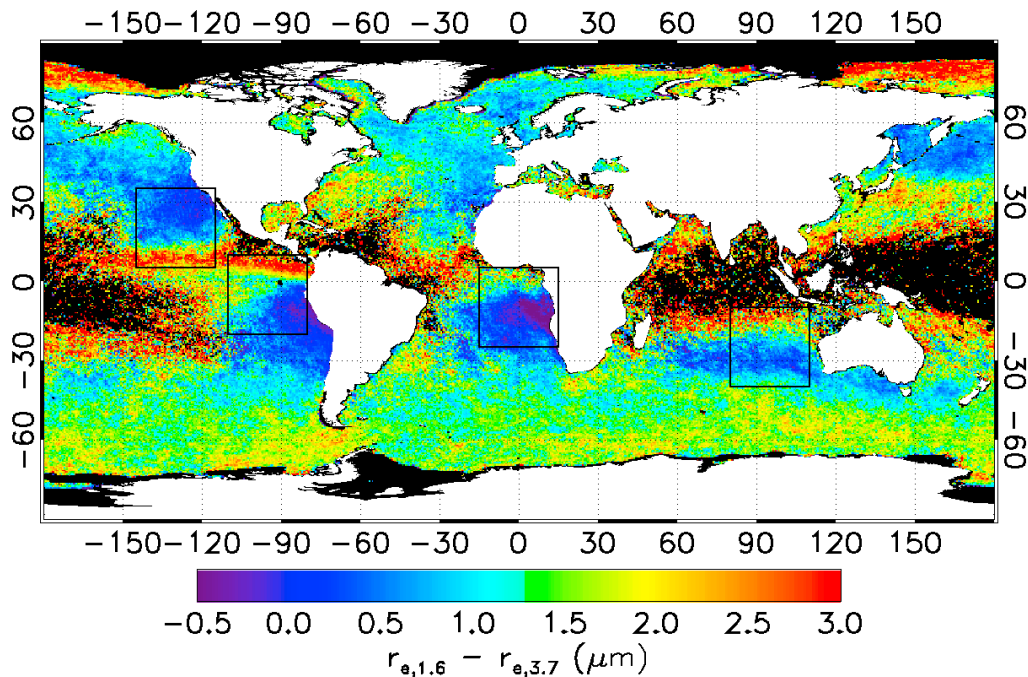


Figure 11. Annual mean effective radius difference between the 1.6 and 3.7 μm MODIS channels for warm nonprecipitating overcast domains. The relationship between LWP bias and effective radius difference in the four marked subregions is plotted in Figure 12.

increasing from cloud base to top but exacerbates microwave-VNIR LWP differences when the droplet profile is neutral or decreasing with height.

[52] In theory, a better approach would be to estimate droplet profile on a case-by-case basis from the three near-infrared MODIS size retrievals. Platnick [2000], however, expressed serious doubts regarding the possibility of such an inversion due to the relatively little difference in the information content of the 1.6 and 2.2 μm bands. Nevertheless, Chen *et al.* [2007] made an attempt to derive linear r_e profiles in a data set limited to 1 day and claimed a small but systematic improvement of $\sim 10\%$ in corresponding VNIR LWPs compared to AMSR-E. Chen *et al.* [2008] further applied this method to data from the East Pacific Investigation of Climate (EPIC) Stratocumulus Study and found that r_e vertically increased in nondrizzling clouds but often decreased in drizzling cases.

[53] Here we only investigated if large-scale LWP bias variations in Figure 6 might be related to variations in cloud vertical stratification but did not derive VNIR LWP corrections. To this effect, we analyzed the geographical distribution of MODIS effective radius differences focusing primarily on the least noisy 1.6–3.7 μm discrepancies. However, in the regional analysis off the Namibian coast we relied on 2.2–3.7 μm differences in order to minimize absorbing aerosol effects, which introduced the largest negative biases in 1.6 μm r_e retrievals [Haywood *et al.*, 2004]. Nominally, negative/positive 1.6–3.7 μm or 2.2–3.7 μm r_e differences would indicate drop sizes increasing/decreasing from cloud base to top.

[54] Annual mean results, given in Figure 11, indicated that the geographic distribution of Δr_e was not random; in the tropics/subtropics it appeared to broadly vary with cloud

type. Marine Sc was characterized by small negative/positive values, which systematically increased to larger positive values in cumuliform cloud regimes. The southern oceans and Arctic regions also showed large positive values, suggesting that undetected cloud top ice might be partially responsible for the observed spatial pattern. In order to reduce possible ice effects, we also made calculations restricted to cloud top temperatures above 273 and 278 K. In both cases, spatial variations were very similar to Figure 11 showing the sharp transitions in the tropics/subtropics.

[55] Contrary to expectations, annual mean Δr_e tended to be mostly positive, even in marine Sc, suggesting a decrease in drop size from cloud base to top. In Sc areas, Δr_e was mostly negative up to $-1 \mu\text{m}$ in boreal summer; in boreal winter, however, it shifted to larger positive values, resulting in small positive annual means. Consequently, although LWP bias was better correlated with Δr_e than with microwave cloud temperature error, the sign of Δr_e could not generally differentiate between MODIS LWP overestimation and underestimation. This is clearly demonstrated in Figure 12, plotting LWP bias as a function of effective radius difference for 1° annual means in our four selected transition regions. As shown, LWP bias switched sign at a positive Δr_e between 0.5 and 1.5 μm instead of near zero. Boreal summer and boreal winter scatterplots were similar but with the former shifted to lower Δr_e by 0.5–1 μm and the latter to larger Δr_e by $\sim 0.5 \mu\text{m}$. As a result, the sign of Δr_e was indicative of that of LWP bias only in boreal summer.

[56] At this point, we do not have an explanation for this puzzling result and can only list a number of potential causes. Although the 3.7 μm band is well calibrated, the complicated separation of thermal and solar components

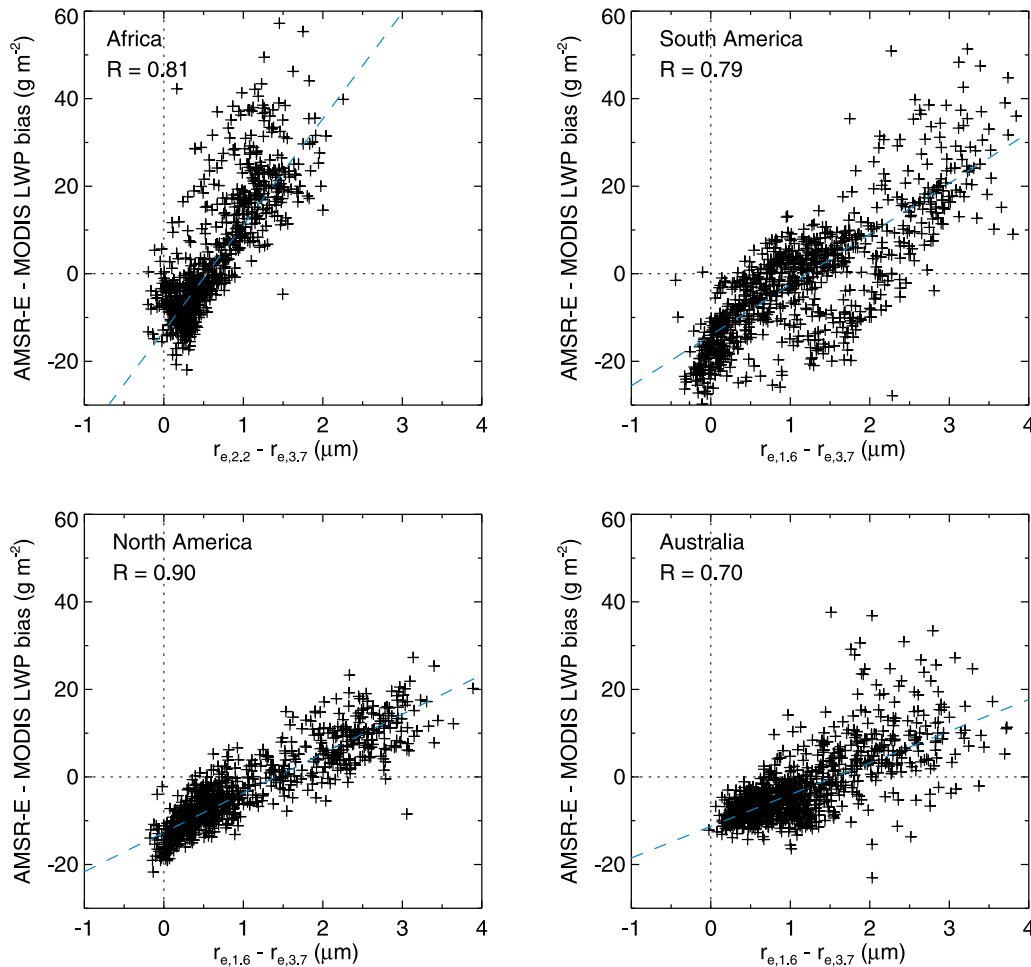


Figure 12. AMSR-E-standard MODIS LWP bias versus MODIS effective radius difference in the four marked regions of Figure 11. Effective radius difference is between the 2.2 and 3.7 μm channels for Africa in order to minimize absorbing aerosol effects; everywhere else it is between the 1.6 and 3.7 μm channels. Data are 1° annual means in warm nonprecipitating overcast clouds, and the correlation coefficients and dashed lines correspond to linear fits.

might introduce r_e retrieval errors. Another possibility is that positive vertical drop size gradients tend to be larger than negative ones, leading to mostly positive average values [Chang and Li, 2003]. Cloud top entrainment might also play a role. Both in situ measurements and large eddy simulations show that a sharp decrease in liquid water content and effective radius could occur in the topmost few dozen meters of Sc clouds due to mixing with drier ambient air [Stevens, 2005]. This drop-off might reduce effective radius retrievals particularly in the 3.7 μm band as its weighting function peaks closest to cloud top.

[57] Concerning entrainment effects, we note that Polarization and Directionality of the Earth's Reflectances (POLDER) drop size estimates in Sc also showed a low bias of $\sim 2 \mu\text{m}$ compared to MODIS 2.2 μm values [Bréon and Doutriaux-Boucher, 2005]. Because the polarization technique is based on single scattering, it is probably even more sensitive to cloud top than the 3.7 μm MODIS channel. Although a satisfactory explanation was not found for the POLDER-MODIS r_e bias either, entrainment mixing was offered as a possible contributing factor. The impact of this effect on MODIS drop size retrievals will have to be

quantified by recalculating near-infrared weighting functions using more realistic vertical profiles than the ones considered by Platnick [2000], which ignored the cloud top drop-off.

[58] As a final note, we warn against overinterpreting the above results. Instantaneous retrievals are noisy and subject to a multitude of possible errors, making it difficult to gauge the exact information content of near-infrared channels regarding cloud stratification. What can be said with some certainty is that in the tropics/subtropics, large-scale variations of AMSR-E-MODIS LWP bias appear associated with Sc to Cu transition, and so do variations of effective radius difference. However, more detailed algorithm sensitivity studies will be needed to establish if this correlation is fortuitous or indeed physical.

4.4. Absorbing Aerosol Effects in MODIS LWP

[59] In this section, we estimate the effect of absorbing aerosols, which can introduce a negative bias in both droplet effective radius and optical thickness, and hence in MODIS LWP, when they reside above low-level clouds. This negative bias in the baseline 2.2 μm effective radius is usually

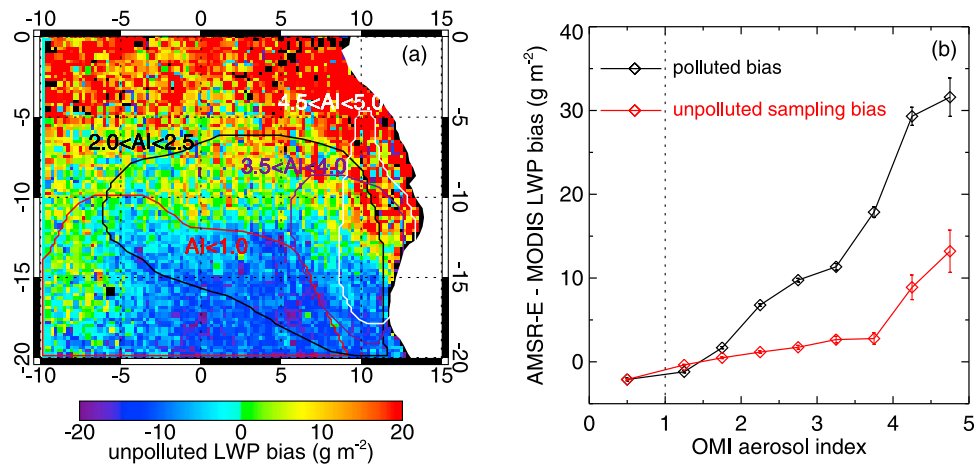


Figure 13. (a) Geographic distribution of AMSR-E-standard MODIS LWP bias in the African biomass smoke region calculated for warm nonprecipitating overcast clouds with Ozone Monitoring Instrument (OMI) Aerosol Index (AI) ≤ 1 and averaged over July–August–September 2007. Contour lines encompass 67% of observations in the given AI bins. (b) LWP bias as a function of aerosol index with bars depicting the standard error of the mean. The black curve represents smoke-affected retrievals, while the red curve is the spatial sampling bias obtained from Figure 13a. Note for the red (“unpolluted”) curve, OMI AI indicates geographic location within the region, rather than actual aerosol load.

less than $1 \mu\text{m}$; however, it can be up to 30% in optical thickness according to calculations by *Haywood et al.* [2004]. *Bennartz* [2007] noted a systematic MODIS LWP underestimation in Sc off southern Africa during the biomass-burning season, which was attributed to overlying absorbing aerosols by *Bennartz and Harshvardhan* [2007]. In the same region and season, *Wilcox et al.* [2009] estimated a domain-mean absorbing aerosol effect of 5.6 g m^{-2} , defined as AMSR-E-MODIS LWP bias for all samples minus that for unpolluted/weakly polluted samples with OMI AI ≤ 1 .

[60] Using this definition, we first estimated the annual global mean absorbing aerosol effect in our data and found it a trivial -1 g m^{-2} . This was not surprising considering that absorbing aerosols are highly seasonal and cover only a small portion of oceans at any given time. Next, we made calculations for the period July–August–September in the study area of *Wilcox et al.* [2009] ($20^{\circ}\text{S}-0^{\circ}$, $10^{\circ}\text{W}-15^{\circ}\text{E}$), which was a subset of our previously defined Africa domain. As shown in Figure 6, this region is characterized by a marked south-north LWP bias gradient, in all seasons and independently of the presence of smoke aerosols. Neglecting this underlying LWP bias pattern could distort estimates of aerosol effect because different AI bins sample different parts of the domain, as demonstrated in Figure 13a for 2007. Here the unpolluted background bias was calculated from cases with AI ≤ 1 , and the contour lines encompass 67% of observations in the given AI bins. The smallest AI bin mostly sampled the southern portion of the domain further out at sea, but as AI increased, sampling moved north and east, closer to shore (the source region). Similar results were obtained for the biomass burning seasons in 2005 and 2006 considered by *Wilcox et al.* [2009], with AI bin locations showing some interannual variations.

[61] The resulting sampling effect is depicted in Figure 13b, which plots domain-mean AMSR-E-standard MODIS LWP bias for AI values 1–5, corresponding to MODIS aerosol

optical depths between 0.1 and 2.1. The black curve shows retrievals actually affected by smoke, while the red curve is the sampling artifact estimated as the average background (unpolluted) LWP bias at the locations of AI measurements in a particular bin. For weakly polluted cases with AI ≤ 1 , the LWP bias was very close to zero due to cancellation of errors between the southern and northern parts of the domain. At higher aerosol loads, however, MODIS increasingly underestimated AMSR-E as a result of reduced cloud optical thickness. (The MODIS LWP underestimation increased with optical thickness in agreement with *Haywood et al.* [2004] and *Wilcox et al.* [2009].) As indicated by the red curve, part of the apparent absorbing aerosol bias was, in fact, caused by larger AI values preferably occurring in areas where MODIS generally underestimated AMSR-E. Neglecting such sampling artifacts, as by *Wilcox et al.* [2009], could lead to overestimating absorbing aerosol effects by 30%–40% at larger AI values.

[62] As shown above, absorbing aerosols can introduce significant VNIR LWP biases at the highest aerosol loads; however, most of our data in Figure 13b were only weakly polluted, resulting in a rather small mean effect. For example, the apparent reduction in domain-mean MODIS LWP during the 2007 biomass burning season was only $\sim 3 \text{ g m}^{-2}$ (average of black curve), which further reduced to slightly below 2 g m^{-2} after sampling issues were accounted for (average of the difference between the black and red curves). The apparent and corrected MODIS underestimations for the 2005–2006 biomass burning season were $4\text{--}5 \text{ g m}^{-2}$ (in reasonable agreement with *Wilcox et al.* [2009]) and $2\text{--}3 \text{ g m}^{-2}$, respectively.

4.5. Cloud-Rain Partitioning Issues in AMSR-E LWP

[63] Up to this point, we only considered nonraining clouds in our comparison. In this section, we extend the analysis to rain flagged cases; however, still excluding broken or ice-contaminated scenes. These criteria yielded a

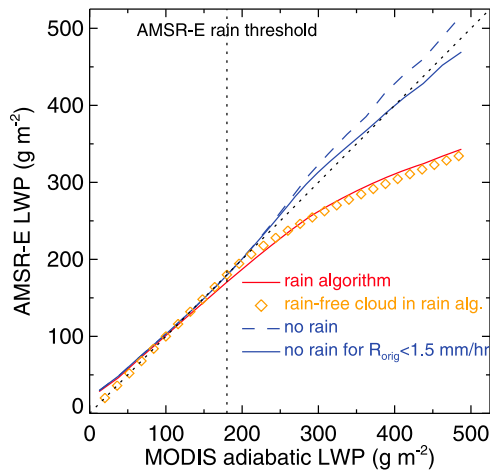


Figure 14. Cloud-rain partitioning effects on AMSR-E-adiabatic MODIS LWP comparison. The solid red curve corresponds to actual retrievals with the operational Wentz rain algorithm. Gold diamonds are estimates of what the rain algorithm would retrieve in rain-free clouds. The blue curves are modified Wentz retrievals with rain removal turned off (1) completely (dashed curve) and (2) only for rain rates below 1.5 mm/hr (solid curve).

further 1.4 million samples but limited rain rates to below 5 mm/hr because higher values were associated with the presence of ice. As explained in section 2.1, rain seriously complicates any microwave retrieval technique because it requires a priori partitioning of total water into cloud and rain components. Specifically, the Wentz algorithm uses a globally fixed rain threshold of 180 g m^{-2} and parameterizes LWP in precipitating clouds as proportional to the square root of rain rate.

[64] In order to gain some insight into the validity of these assumptions, we evaluated AMSR-E LWP as a function of MODIS adiabatic LWP for the combined (rain-free plus rain flagged) data set. (We used adiabatic MODIS retrievals as reference here because they are unbiased compared to AMSR-E in a global mean sense.) Annual results are plotted in Figure 14 by the solid red curve, showing quite good agreement between microwave and VNIR estimates up to the rain threshold, above which, however, AMSR-E increasingly underestimated MODIS. The mean underestimation reached $\sim 150 \text{ g m}^{-2}$ (or 30%) at the largest MODIS LWPs.

[65] What could cause these discrepancies? As noted earlier, MODIS increasingly overestimated AMSR-E at larger solar zenith angles, particularly in heterogeneous clouds, which could produce qualitatively similar results. Prompted by this, we made separate calculations for the most heterogeneous and most homogeneous third of clouds. In heterogeneous cases, retrievals started to diverge at a slightly smaller LWP, while in homogeneous cases the divergence occurred at a somewhat larger LWP; otherwise results were comparable and stayed within $\pm 30 \text{ g m}^{-2}$ of the overall average (red curve). Furthermore, *Wilcox et al.* [2009] found similar AMSR-E underestimations at lower latitudes as well, where MODIS heterogeneity effects were generally reduced. These findings suggested that VNIR

heterogeneity effects alone could not explain the observed discrepancies.

[66] The fact that microwave and VNIR estimates started to diverge above the rain threshold LWP pointed to possible cloud-rain partitioning issues in AMSR-E retrievals. A relatively low precipitation threshold means that part of the water content of thicker rain-free clouds might be erroneously assigned to rain. In fact, CloudSat retrievals indicate only $\sim 30\%$ probability of precipitation in warm clouds at an LWP of $180\text{--}200 \text{ g m}^{-2}$ [*Lebsock et al.*, 2008]. This suggests that a significant portion of rain flagged AMSR-E retrievals might actually be rain-free, and as such, subject to the above error. (It should be noted, however, that a large number of low-level liquid clouds are below the detection limit of the CloudSat radar or are otherwise missed due to surface contamination.)

[67] We investigated the effect of rain removal by estimating what LWP the operational AMSR-E algorithm would retrieve in rain-free clouds above the precipitation threshold (see gold diamonds in Figure 14). These estimates were derived from the governing equations in section 2.1 and confirmed the observed biases: an increasing portion of the water content of thicker rain-free clouds was assigned to precipitation. Obviously, a fraction of clouds with LWP between 180 and 500 g m^{-2} bound to precipitate; thus, the excellent fit between rain-free cloud estimates and actual observations must also have been due to the presence of additional biases (liquid temperature error, heterogeneity effects, etc.). Nevertheless, these results demonstrated the general effect of cloud-rain partitioning errors.

[68] As a further step, Remote Sensing Systems reprocessed our boreal summer and boreal winter data with rain removal completely turned off. These modified AMSR-E LWPs, indicated by the dashed blue line, compared considerably better with MODIS LWPs but now exhibited slight overestimations. We found the best agreement between microwave and VNIR estimates when rain removal was only turned off for rain rates below 1.5 mm/hr, as shown by the solid blue line. Taken together, these findings suggested that the 180 g m^{-2} precipitation threshold was too low, at least in a global mean sense.

[69] Finally, we note that the Wentz algorithm is tuned to produce reasonable rain rates and rain coverage in comparison with other well-known precipitation climatologies. It might be impossible to optimize the algorithm simultaneously for LWP and rain. However, a separate product specifically minimizing discrepancies with MODIS LWPs could be introduced. Alternatively, rain removal could be turned off entirely in order to retrieve total (cloud plus rain) water path, which is the quantity microwave techniques are ultimately sensitive to. This could facilitate more straightforward comparisons with climate models by eliminating differences due to dissimilar cloud-rain partitioning in models and satellite retrievals.

5. Summary

[70] We analyzed 1 year of AMSR-E Wentz and MODIS cloud liquid water path estimates, representing the current state of the art in microwave and VNIR retrievals. The comparison was made over the global oceans on a quarter-degree scale and only included warm clouds in order to

avoid ambiguities due to ice; however, both standard (vertically homogeneous) and adiabatically stratified MODIS LWPs were evaluated. Our goal was to characterize microwave-VNIR LWP differences in a statistically robust data set and identify their potential causes for future studies. Main findings are summarized as follows.

[71] When all scenes were considered, AMSR-E overestimated MODIS by 45% on average, and retrievals were only moderately correlated, with a coefficient of 0.74 and RMS difference of 41 g m^{-2} . However, we found the microwave-VNIR comparison to be strongly dependent on cloud fraction and geographic location. In overcast scenes, estimates were generally better correlated at 0.83, but with significant regional variations. The relationship between the techniques was loosest at high latitudes above 55° and tightest in marine Sc regions with correlations up to 0.95 and typical RMS differences of $10\text{--}20 \text{ g m}^{-2}$. Overcast domains were also characterized by a MODIS high bias. In broken scenes, on the other hand, AMSR-E increasingly overestimated MODIS and retrievals became gradually uncorrelated as cloud fraction decreased below 80%.

[72] Although we could not fully explain this microwave high bias at low cloud fractions, we noted a global mean AMSR-E LWP bias of 12 g m^{-2} in cloud-free scenes as well. This clear-sky microwave bias showed systematic geographic variations, being smallest in colder marine Sc regions and largest over warm oceans. In addition, the AMSR-E clear-sky bias and low-cloud-fraction bias both had similar dependencies: a negative correlation with surface wind speed and a weaker positive correlation with water vapor. These results suggested that uncertainties in surface emission and gaseous absorption models were partly responsible for Wentz overestimation in thin broken clouds.

[73] The remainder of the study focused exclusively on overcast domains. In this subset, the global annual mean MODIS overestimation of $\sim 17\%$ could be almost completely eliminated by adiabatic correction, which worked equally well on monthly time scales, with MODIS global means being within 5 g m^{-2} (or 6%) of AMSR-E means. However, the excellent mean performance of the adiabatic model masked significant regional differences. Zonal means showed AMSR-E overestimation between $45^\circ\text{S}\text{--}45^\circ\text{N}$, and rapidly increasing MODIS overestimation at higher latitudes, particularly in the winter hemisphere. This was the result of strikingly different latitudinal variations in LWP, whereby AMSR-E generally decreased but MODIS increased toward the poles.

[74] In the tropics/subtropics, the AMSR-E-MODIS LWP bias also showed systematic variations with cloud regimes. In marine Sc regions, MODIS overestimated AMSR-E, while in areas frequented by cumuliform clouds, the reverse was true. This resulted in large-scale coherent spatial patterns in LWP bias wherever Sc transitioned into trade wind Cu. Most notably, there were marked zonal LWP bias gradients at the Pacific Cold Tongue and in an extensive area stretching from the Namibian coast to the Gulf of Guinea.

[75] Prompted by the existence of systematic LWP bias variations in the African Sc region, generally regarded as a test bed of aerosol-cloud interactions, we estimated absorbing aerosol effects on VNIR retrievals. In a global annual mean sense, absorbing aerosols introduced a trivial (-1 g m^{-2}) low bias in MODIS LWPs. The regional-mean

bias during the biomass-burning season was only slightly larger at -3 to -5 g m^{-2} , although locally it could be as high as -30 g m^{-2} in heavily polluted areas. However, 30%–40% of the apparent absorbing aerosol bias could be attributed to sampling artifacts due to systematic zonal variations in AMSR-E-MODIS LWP difference. These results implied that neglecting persistent geographic variations in the background (unpolluted) microwave-VNIR LWP bias could lead to overestimating aerosol effects in VNIR retrievals.

[76] In pursuit of an explanation for the increasing MODIS overestimation at high latitudes, we analyzed the solar zenith angle dependence of microwave and VNIR retrievals. Up to a SZA of 35° the techniques showed good agreement; at lower Sun, however, they diverged: AMSR-E leveled off, but MODIS rapidly increased with SZA driven by an increase in cloud optical thickness. In addition, while the SZA dependence of microwave estimates was relatively insensitive to scene type, the increase in MODIS LWPs with SZA was significantly larger in heterogeneous than in homogeneous clouds. Only in the most homogeneous clouds did VNIR LWPs show SZA dependence qualitatively similar to microwave LWPs. These findings suggested that microwave-VNIR differences at high latitudes were largely due to 3-D effects in 1-D MODIS retrievals over heterogeneous clouds at low Sun.

[77] Such heterogeneity effects were significantly reduced at lower latitudes; hence, they were unlikely to play a major role in the emergence of the coherent tropical LWP bias patterns. A more likely candidate was systematic errors in the Wentz cloud temperature parameterization, which we evaluated against MODIS cloud top temperatures. Although the global mean cloud temperature bias was only -1.5°C , regional errors were as high as $\pm 6^\circ\text{C}$ and showed geographic variations similar to LWP bias variations. In marine Sc (over colder oceans) the Wentz parameterization underestimated, while in cumuliform clouds (over warmer oceans) overestimated liquid temperature, resulting in moderately strong ($R = 0.6\text{--}0.8$) large-scale correlations between temperature error and LWP bias in Sc transition regions.

[78] Systematic errors in standard MODIS LWP due to geographic variations in vertical cloud stratification might have also contributed to the tropical LWP bias patterns. Although the adiabatic model removed the MODIS high bias in a global mean sense, regionally it represented an improvement in marine Sc only, while exacerbated differences in cumuliform clouds where standard MODIS generally underestimated AMSR-E. Motivated by this, we investigated if MODIS effective radius difference offered some clues about vertical cloud stratification. We found that *relative* variations in $1.6\text{--}3.7 \mu\text{m}$ effective radius difference also showed similar large-scale patterns as microwave-VNIR LWP bias, resulting in significant correlations ($R = 0.7\text{--}0.9$) between the quantities. However, effective radius difference was mostly positive; thus, its sign was generally a poor indicator of the sign of LWP bias. We realize that interpreting the information content of MODIS near-infrared channels is rather ambiguous; nevertheless, we believe these apparent large-scale correlations do warrant further study.

[79] Finally, we investigated cloud-rain partitioning uncertainties in Wentz retrievals, prompted by the fact that AMSR-E increasingly underestimated MODIS at LWPs

above the microwave precipitation threshold. The fixed rain threshold of only 180 g m^{-2} resulted in a significant number of rain-free clouds being processed as raining clouds. We found that the AMSR-E low bias could be well explained by the Wentz algorithm erroneously assigning an increasing portion of the liquid water content of such clouds to precipitation. In fact, when rain retrieval was completely turned off, AMSR-E LWPs compared significantly better with MODIS values, but now exhibited slight overestimations. The agreement between microwave and VNIR estimates was best when rain removal was only turned off for rain rates below 1.5 mm/hr . Taken together, these findings indicated that the Wentz precipitation threshold was too low.

[80] Of the potential error sources listed above, the ones affecting microwave retrievals appear somewhat easier to tackle. The sensitivity of Wentz LWPs to cloud temperature uncertainties could be straightforwardly evaluated by replacing the current parameterization with MODIS cloud top temperatures. Some progress could also be made in deriving a more realistic cloud-rain partitioning formulation, either from CloudSat retrievals or cloud-resolving models. Quantifying and correcting for VNIR retrieval errors due to heterogeneity effects or cloud vertical stratification remain significantly more challenging. Perhaps a statistical inversion technique utilizing 3-D radiative transfer calculations in a large number of simulated cloud fields offers the best hope to handle such errors in an operational context.

[81] **Acknowledgments.** This work was partially supported by the European Commission's Marie Curie Actions under grant agreement MIRG-CT-2007-208245. AMSR-E data are produced by Remote Sensing Systems and sponsored by the NASA Earth Science MEASURES DISCOVER Project and the AMSR-E Science Team. Data are available at <http://www.remss.com>. We thank Kyle Hilburn for reprocessing AMSR-E retrievals and Paquita Zuidema, Stefan Kinne, and three anonymous reviewers for suggestions that greatly improved the quality of the paper.

References

- Bennartz, R. (2007), Global assessment of marine boundary layer cloud droplet number concentration from satellite, *J. Geophys. Res.*, *112*, D02201, doi:10.1029/2006JD007547.
- Bennartz, R., and Harshvardhan (2007), Correction to "Global assessment of marine boundary layer cloud droplet number concentration from satellite", *J. Geophys. Res.*, *112*, D16302, doi:10.1029/2007JD008841.
- Bony, S., and J.-L. Dufresne (2005), Marine boundary layer clouds at the heart of tropical cloud feedback uncertainties in climate models, *Geophys. Res. Lett.*, *32*, L20806, doi:10.1029/2005GL023851.
- Borg, L. A., and R. Bennartz (2007), Vertical structure of stratiform marine boundary layer clouds and its impact on cloud albedo, *Geophys. Res. Lett.*, *34*, L05807, doi:10.1029/2006GL028713.
- Bréon, F.-M., and M. Doutriaux-Boucher (2005), A comparison of cloud droplet radii measured from space, *IEEE Trans. Geosci. Remote Sens.*, *43*, 1796–1805, doi:10.1109/TGRS.2005.852838.
- Cahalan, R. F., W. Ridgway, W. J. Wiscombe, T. L. Bell, and J. B. Snider (1994), The albedo of fractal stratocumulus clouds, *J. Atmos. Sci.*, *51*, 2434–2455, doi:10.1175/1520-0469(1994)051<2434:TAOFSC>2.0.CO;2.
- Chang, F.-L., and Z. Li (2003), Retrieving vertical profiles of water-cloud droplet effective radius: Algorithm modification and preliminary application, *J. Geophys. Res.*, *108*(D24), 4763, doi:10.1029/2003JD003906.
- Chen, R., F.-L. Chang, Z. Li, R. Ferraro, and F. Weng (2007), Impact of the vertical variation of cloud droplet size on the estimation of cloud liquid water path and rain detection, *J. Atmos. Sci.*, *64*, 3843–3853, doi:10.1175/2007JAS126.1.
- Chen, R., R. Wood, Z. Li, R. Ferraro, and F.-L. Chang (2008), Studying the vertical variation of cloud droplet effective radius using ship and spaceborne remote sensing data, *J. Geophys. Res.*, *113*, D00A02, doi:10.1029/2007JD009596.
- Cornet, C., J.-C. Buriez, J. Riédi, H. Isaka, and B. Guillemet (2005), Case study of inhomogeneous cloud parameter retrieval from MODIS data, *Geophys. Res. Lett.*, *32*, L13807, doi:10.1029/2005GL022791.
- Evans, K. F., A. Marshak, and T. Várnai (2008), The potential for improved boundary layer cloud optical depth retrievals from the multiple directions of MISR, *J. Atmos. Sci.*, *65*, 3179–3196, doi:10.1175/2008JAS2627.1.
- Greenwald, T. J., S. A. Christopher, and J. Chou (1997), Cloud liquid water path comparisons from passive microwave and solar reflectance satellite measurements: Assessment of sub-field-of-view clouds effects in microwave retrievals, *J. Geophys. Res.*, *102*, 19,585–19,596, doi:10.1029/97JD01257.
- Greenwald, T. J., T. S. L'Ecuyer, and S. A. Christopher (2007), Evaluating specific error characteristics of microwave-derived cloud liquid water products, *Geophys. Res. Lett.*, *34*, L22807, doi:10.1029/2007GL031180.
- Haywood, J. M., S. R. Osborne, and S. J. Abel (2004), The effect of overlying absorbing aerosol layers on remote sensing retrievals of cloud effective radius and cloud optical depth, *Q. J. R. Meteorol. Soc.*, *130*, 779–800, doi:10.1256/qj.03.100.
- Hilburn, K. A., and F. J. Wentz (2008), Intercalibrated passive microwave rain products from the Unified Microwave Ocean Retrieval Algorithm (UMORA), *J. Appl. Meteorol. Climatol.*, *47*, 778–794, doi:10.1175/2007JAMC1635.1.
- Horváth, Á., and R. Davies (2004), Anisotropy of water cloud reflectance: A comparison of measurements and 1D theory, *Geophys. Res. Lett.*, *31*, L01102, doi:10.1029/2003GL018386.
- Horváth, Á., and R. Davies (2007), Comparison of microwave and optical cloud water path estimates from TMI, MODIS, and MISR, *J. Geophys. Res.*, *112*, D01202, doi:10.1029/2006JD007101.
- Horváth, Á., and C. Gentemann (2007), Cloud-fraction-dependent bias in satellite liquid water path retrievals of shallow, non-precipitating marine clouds, *Geophys. Res. Lett.*, *34*, L22806, doi:10.1029/2007GL030625.
- Lafont, D., and B. Guillemet (2004), Subpixel fractional cloud cover and inhomogeneity effects on microwave beam-filling error, *Atmos. Res.*, *72*, 149–168, doi:10.1016/j.atmosres.2004.03.013.
- Lebsock, M. D., G. L. Stephens, and C. Kummerow (2008), Multisensor satellite observations of aerosol effects on warm clouds, *J. Geophys. Res.*, *113*, D15205, doi:10.1029/2008JD009876.
- Loeb, N. G., and J. A. Coakley Jr. (1998), Inference of marine stratus cloud optical depths from satellite measurements: Does 1D theory apply? *J. Clim.*, *11*, 215–233, doi:10.1175/1520-0442(1998)011<0215:1OMSCO>2.0.CO;2.
- Loeb, N. G., and R. Davies (1996), Observational evidence of plane parallel model biases: Apparent dependence of cloud optical depth on solar zenith angle, *J. Geophys. Res.*, *101*, 1621–1634, doi:10.1029/95JD03298.
- Loeb, N. G., T. Várnai, and D. M. Winker (1998), Influence of subpixel-scale cloud-top structure on reflectances from overcast stratiform cloud layers, *J. Atmos. Sci.*, *55*, 2960–2973, doi:10.1175/1520-0469(1998)055<2960:IOSSCT>2.0.CO;2.
- Marshak, A., S. Platnick, T. Várnai, G. Wen, and R. F. Cahalan (2006), Impact of three-dimensional radiative effects on satellite retrievals of cloud droplet sizes, *J. Geophys. Res.*, *111*, D09207, doi:10.1029/2005JD006686.
- Nakajima, T., and M. D. King (1990), Determination of the optical thickness and effective particle radius of clouds from reflected solar radiation measurements. Part I: Theory, *J. Atmos. Sci.*, *47*, 1878–1893, doi:10.1175/1520-0469(1990)047<1878:DOTOTA>2.0.CO;2.
- O'Dell, C. W., F. J. Wentz, and R. Bennartz (2008), Cloud liquid water path from satellite-based passive microwave observations: A new climatology over the global oceans, *J. Clim.*, *21*, 1721–1739, doi:10.1175/2007JCLI1958.1.
- Oreopoulos, L., and R. F. Cahalan (2005), Cloud inhomogeneity from MODIS, *J. Clim.*, *18*, 5110–5124, doi:10.1175/JCLI3591.1.
- Platnick, S. (2000), Vertical photon transport in cloud remote sensing problems, *J. Geophys. Res.*, *105*, 22,919–22,935, doi:10.1029/2000JD900333.
- Platnick, S., M. D. King, S. A. Ackerman, W. P. Menzel, B. A. Baum, J. C. Riedi, and R. A. Frey (2003), The MODIS cloud products: Algorithms and examples from Terra, *IEEE Trans. Geosci. Remote Sens.*, *41*, 415–473, doi:10.1109/TGRS.2002.808301.
- Stevens, B. (2005), Atmospheric moist convection, *Annu. Rev. Earth Planet. Sci.*, *33*, 605–643, doi:10.1146/annurev.earth.33.092203.122658.
- Torres, O., A. Tanskanen, B. Veihelmann, C. Ahn, R. Braak, P. K. Bhartia, P. Veehkind, and P. Levelt (2007), Aerosols and surface UV products from Ozone Monitoring Instrument observations: An overview, *J. Geophys. Res.*, *112*, D24S47, doi:10.1029/2007JD008809.
- Turner, D. D., et al. (2007), Thin liquid water clouds: Their importance and our challenge, *Bull. Am. Meteorol. Soc.*, *88*(2), 177–190, doi:10.1175/BAMS-88-2-177.

- Várnai, T., and A. Marshak (2001), Statistical analysis of the uncertainties in cloud optical depth retrievals caused by three-dimensional radiative effects, *J. Atmos. Sci.*, *58*, 1540–1548, doi:10.1175/1520-0469(2001)058<1540:SAOTUI>2.0.CO;2.
- Várnai, T., and A. Marshak (2007), View angle dependence of cloud optical thicknesses retrieved by Moderate Resolution Imaging Spectroradiometer (MODIS), *J. Geophys. Res.*, *112*, D06203, doi:10.1029/2005JD006912.
- Wentz, F. J. (1997), A well-calibrated ocean algorithm for special sensor microwave/imager, *J. Geophys. Res.*, *102*, 8703–8718, doi:10.1029/96JC01751.
- Wentz, F. J., and T. Meissner (2000), AMSR ocean algorithm, version 2, *RSS Tech. Rep. 121599A-1*, 66 pp., Remote Sens. Syst., Santa Rosa, California.
- Wentz, F. J., and R. Spencer (1998), SSM/I rain retrievals within a unified all-weather ocean algorithm, *J. Atmos. Sci.*, *55*, 1613–1627, doi:10.1175/1520-0469(1998)055<1613:SIRRWA>2.0.CO;2.
- Wilcox, E. M., Harshvardhan, and S. Platnick (2009), Estimate of the impact of absorbing aerosol over cloud on the MODIS retrievals of cloud optical thickness and effective radius using two independent retrievals of liquid water path, *J. Geophys. Res.*, *114*, D05210, doi:10.1029/2008JD010589.
- Wood, R., and D. L. Hartmann (2006), Spatial variability of liquid water path in marine low cloud: The importance of mesoscale cellular convection, *J. Clim.*, *19*, 1748–1764, doi:10.1175/JCLI3702.1.
- Zhao, G., and L. Di Girolamo (2006), Cloud fraction errors for trade wind cumuli from EOS-Terra instruments, *Geophys. Res. Lett.*, *33*, L20802, doi:10.1029/2006GL027088.
- Zuidema, P., E. Westwater, C. Fairall, and D. Hazen (2005), Ship-based liquid water path estimates in marine stratocumulus, *J. Geophys. Res.*, *110*, D20206 doi:10.1029/2005JD005833.
-
- Á. Horváth and C. Seethala, Max Planck Institute for Meteorology, Bundesstrasse 53, D-20146 Hamburg, Germany. (seethala.chellappan@zmaw.de)